NASA TECHNICAL NOTE

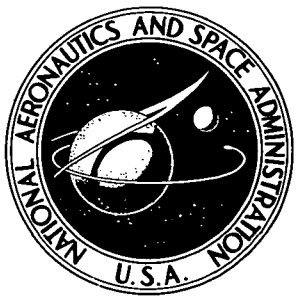

NASA TN D-7319

NASA TN D-7319

A LABORATORY SIMULATION OF A SINGLE-AXIS DUAL-LEVEL PRECISION POINTING SYSTEM

by Gordon F. Bullock, Frederick R. Morrell, and K. C. Romanczyk

Langley Research Center
Hampton, Va. 23665

NATIONAL AERONAUTICS AND SPACE ADMINISTRATION • WASHINGTON, D. C. • OCTOBER 1973

1. Report No.	2. Government Accession No.	3. Recipient's Catalog No.
NASA TN D-7319		

4. Title and Subtitle	5. Report Date
A LABORATORY SIMULATION OF A SINGLE-AXIS DUAL-LEVEL PRECISION POINTING SYSTEM	October 1973
	6. Performing Organization Code

7. Author(s)	8. Performing Organization Report No.
Gordon F. Bullock, Frederick R. Morrell, and K. C. Romanczyk	L-8943
	10. Work Unit No.
9. Performing Organization Name and Address	188-78-57-05
NASA Langley Research Center Hampton, Va. 23665	11. Contract or Grant No.
	13. Type of Report and Period Covered
12. Sponsoring Agency Name and Address	Technical Note
National Aeronautics and Space Administration Washington, D.C. 20546	14. Sponsoring Agency Code

15. Supplementary Notes

16. Abstract

The laboratory simulation of a scaled single-axis dual-level control system for a large space telescope is demonstrated. The dual-level control system consists of a coarse-body-pointing system and a fine-pointing system, which uses an image motion compensator, an image dissector tube, and digital electronics. The results of the simulation indicate that the dual-level system can be used to provide tracking capability within one-tenth of a diffraction-limited image diameter of a 3-meter f/100 telescope for stars up to a +12.3 visual magnitude.

17. Key Words (Suggested by Author(s))	18. Distribution Statement
Image motion compensator Two-mirror technique Air-bearing simulation Dual-level control	Unclassified – Unlimited

19. Security Classif. (of this report)	20. Security Classif. (of this page)	21. No. of Pages	22. Price*
Unclassified	Unclassified	34	Domestic, $3.00 Foreign, $5.50

*For sale by the National Technical Information Service, Springfield, Virginia 22151

A LABORATORY SIMULATION OF A SINGLE-AXIS DUAL-LEVEL PRECISION POINTING SYSTEM

By Gordon F. Bullock, Frederick R. Morrell,
and K. C. Romanczyk
Langley Research Center

SUMMARY

The laboratory simulation of a scaled single-axis dual-level control system for a large space telescope is demonstrated. The dual-level control system consists of a coarse-body-pointing system and a fine-pointing system, which uses an image motion compensator, an image dissector tube, and digital electronics. The results of the simulation indicate that the dual-level system can be used to provide tracking capability within one-tenth of a diffraction-limited image diameter of a 3-meter f/100 telescope for stars up to a +12.3 visual magnitude.

INTRODUCTION

The resolution advantage of space-based astronomical telescopes over earthbound instruments has been recognized by the scientific community for many years. The resolution of orbiting telescopes, and therefore the required vehicle pointing accuracy, is primarily determined by the point image spread function of the optics. If a 3-meter diffraction-limited telescope is assumed, the resolution would be approximately 0.04 arc second; this would require a vehicle pointing accuracy of 0.01 to 0.005 arc second (ref. 1). The capability to provide this pointing accuracy on the focal plane of the telescope is a significant problem. One technique (ref. 2) suggests the use of a dual-level control system which maintains relatively coarse-vehicle-pointing accuracy while smaller optical elements in the optical train of the telescope maintain the required pointing accuracy (refs. 3 and 4).

This paper reports on the laboratory simulation of a single-axis dual-level pointing control system. The simulation is scaled to provide correct optical and dynamical conditions and is used to provide a parametric analysis of the effects of star image diameter and magnitude and fine-pointing control-system bandwidth on the pointing accuracy of the system. Detailed descriptions and operations of the components of the dual-level system are given in the references.

SYMBOLS

Values are given in both SI and U.S. Customary Units. The measurements and calculations were made in U.S. Customary Units.

D	gyro damping, $\frac{\text{newton-meter-seconds}}{\text{radian}}$ $\left(\frac{\text{foot-pound-seconds}}{\text{radian}}\right)$
H	gyro momentum storage capability, newton-meter-seconds (foot-pound-seconds)
I_g	gyro gimbal inertia, kilogram-meters^2 (slug-feet^2)
I_v	vehicle moment of inertia, kilogram-meters^2 (slug-feet^2)
K	inertial scale factor
S	Laplacian operator, second^{-1}
T_c	gyro control torque, newton-meters (foot-pounds)
T_d	disturbance torque, newton-meters (foot-pounds)
t_1	count up time, seconds
t_2	count down time, seconds
α	gyro gimbal angle, radians
θ_e	instantaneous position error, radians
θ_m	image motion compensator (IMC) mirror position, degrees
θ_v	telescope position, radians
$\dot{\theta}_v$	telescope rate, radians/second

DESCRIPTION OF SIMULATION EQUIPMENT

The dual-level control system consists of the coarse- and the fine-pointing control systems. A brief description of the dual-level system and each individual system is given in this section.

A simplified block diagram of the dual-level system is shown in figure 1. A disturbance torque acting on the vehicle causes a change in telescope attitude which is detected by the coarse- and fine-pointing sensors. The control moment gyro provides a control torque to counteract the disturbance torque and stabilize the telescope within the coarse requirements. The fine control system operates within the coarse-pointing limits to keep the star image fixed on the optical focal plane.

A digital computer is used in the simulation to monitor the system parameters and to make decisions such as selecting the optimum field of view for the fine sensor and unloading the control moment gyro gimbals. An analog computer not shown in the figure is used for signal conditioning purposes. A reaction-control jet system is used for unloading the control moment gyro and for applying disturbance torques to the coarse system.

Coarse System

Control moment gyro (CMG).- The control moment gyro (ref. 5) shown in figure 2 is the twin-rotor single-degree-of-freedom type in which cross-axis coupling is eliminated. The CMG was designed and built with provisions made for varying the gimbal inertia and gyro damping. The effective gimbal inertia can be varied between 0.1357 and 0.2714 kg-m^2 (0.1 and 0.2 slug-ft^2). Gyro damping can be varied between 0.61 and 1.22 $\frac{\text{N-m-sec}}{\text{rad}}$ $\left(0.45 \text{ and } 0.90 \frac{\text{ft-lb-sec}}{\text{rad}}\right)$.

Each rotor has a momentum storage capability of 6.03 N-m-sec (4.45 ft-lb-sec) when driven by a 445-Hz power source. Provisions were made to change the momentum storage capability by varying the frequency of the drive power. The two rotors are mechanically coupled through a 1:1 gear ratio. A servomotor is used to drive the gimbals through an 80:1 gear head. Stall torque of the servomotor is 0.0102 N-m (1.45 in-oz); a flywheel of 0.001356 kg-m^2 (0.001 slug-ft^2) attached to the servomotor represents the inertia seen by the servomotor. An 0.085 N-m (12 in-oz) negator spring is used on one of the gimbals to take up the backlash in the 1:1 gearing and in the 80:1 gear head.

Star sensor.- The star sensor is the reflective beam-splitter type as shown in figure 3. Light from the star entering the lens is focused on the beam splitter. From the beam splitter the light is directed to the two photomultiplier tubes located on each side of the beam splitter. Angular motion of the star with respect to the sensor causes more light

to be directed to one of the photomultiplier tubes. The outputs of the two photomultiplier tubes are subtracted to get the error signal. These photomultiplier tubes were selected and calibrated to give the sensor an output of 2060 volts per radian, the sensor gain required by the model gyro rate loop.

Vehicle inertia simulator.- The air bearing, which is a three-axis vehicle inertia simulator used in a single-axis configuration, is shown in figure 4 with the CMG and control-system hardware mounted on the payload table. The simulator is supported at the center by a ball-and-socket type of low-friction air bearing and the payload table is mounted on a shaft attached to the ball. A journal air bearing is used to restrict the simulator to motion about its vertical axis. The moment of inertia about the simulator vertical axis represents the pitch axis of the telescope in the simulation. Power and signals to the simulator are channeled through a mercury-bath type of slipring assembly.

A block diagram of a typical single-axis coarse control system is shown in figure 5. In this system a disturbance torque T_d acting on the vehicle causes changes in the vehicle body rate $\dot{\theta}_V$ and position θ_V. The change in body rate is sensed by the gyro through gyroscopic cross-coupling torque. The change in position is detected by the coarse star sensor, which sends an error signal to the control moment gyro torquer. This error signal is amplified in the gyro electronics to drive the gyro gimbals. This changes the gyro rotor's momentum vector to generate a torque T_c opposite to the disturbance.

Fine-Pointing System

The fine-pointing system consists of an image motion compensator, an image dissector tube, and digital electronics (refs. 3 and 4). A simplified block diagram of the fine system is shown in figure 6. The image dissector is shown schematically at the top of figure 7. The operation of the system is as follows. The star image is focused on the front face of the tube which is located on the telescope focal plane. The defining aperture, a slit for the single-axis case, is centered in the electron focal plane. The electron image is scanned vertically across the slit by applying a triangular sweep signal to the magnetic deflection coils. In figure 7 the sweep signal is plotted on the upper trace with the vertical axis representing the electron image position and the horizontal axis representing time. The star is off axis; therefore, the path of the electron image is not centered about the slit aperture. When the electron image crosses the slit, an electrical pulse is generated. The pulses are shown idealized in the lower part of the figure. The time interval between successive pulses is measured and the difference between the two times is proportional to the angular error between the star and the telescope. The sign of the resulting number indicates direction. Other symmetrical curves could have been used for the sweep signal; however, the triangular sweep was selected because of its linearity.

The processing of the pulse train is shown in figure 8. The pulses that contain noise are first amplified and then filtered. The principal effect of the filter is to lower the noise bandwidth of the system. The leading and trailing edges of the pulses are then detected by a Schmitt trigger, thereby producing a squared pulse. Both edges of the signal pulse are detected to minimize errors due to noise.

The output of the Schmitt trigger, in conjunction with the sweep frequency signal, controls logic gates which determine the direction of an up-down counter. These gates also provide passage for the clock pulses going to the counter. The up-down counter operates in the up mode during time t_1 and in the down mode during time t_2. At the end of a complete counting period, the resulting digital number $(t_1 - t_2)$ is shifted to the output register.

The fine-pointing control system was designed to operate in five different fields of view. The fields of view are numbered 1 to 5, with 1 or cage being the widest field of view and the least sensitive and 5 being the narrowest field of view and the most sensitive. The field of view is changed by varying the amplitude of the triangular sweep signal. The coarse system drives the telescope to bring the star within the field of view of the fine control system. With no star in the field of view the fine control system is in the cage (1) position. When the star appears in the field of view, the digital computer switches the system into field of view 2. The mirrors of the image motion compensator are then driven by the controller indicated in figure 6 in a direction to bring the star image to the zero error position (ref. 6). The digital computer continuously monitors the star position error and commands fields of view 3, 4, and 5. This generally happens so fast that the system appears to go from cage to field of view 5 instantaneously.

Modifications to fine-pointing system.- In tracking dim stars (13th magnitude or dimmer) with the fine-pointing system two problems were encountered as a result of the small signal-to-noise ratio. First, random pulses generated by noise enter the logic circuitry and generate false error signals. This effect can be pictured by looking at figure 8 and visualizing a noise spike, between the three pulses shown, large enough to reach the threshold level to generate a pulse. The counter would then count up or down on this pulse rather than the one shown. Second, a true pulse may be missed entirely in some instances where the noise may have a canceling effect on the pulse when the noise is opposite polarity to the pulse.

To alleviate the first problem, an electronic window was included in the logic of the fine-pointing system. Figure 9 shows the relationship between the window and the pulse train. The function of the electronic window is to allow only the pulses that occur during the time that the window is open to pass, similar to radar range gate. The upper two traces in figure 9 show that a Schmitt trigger output is generated each time the noise level

exceeds the threshold level of the Schmitt trigger. The lower trace, however, shows that only the pulses generated during the time that the electronic window is open are allowed to pass into the logic gate.

In the second problem, if the noise is of a polarity that causes the pulse not to reach the threshold level of the Schmitt trigger, the counter would continue to count in the same direction until the next detected pulse, thereby resulting in a large error signal. To resolve this problem, a logic circuit was added to detect the absence of a pulse and to cancel that number and transfer a zero to the output register. Should acquisition be lost, a pulse counter was added to cage the system when a prescribed number of consecutive pulses were not detected.

Image motion compensator (IMC).- The purpose of the image motion compensator is to maintain the star image fixed on the focal plane of the telescope despite small motions between the guide star and the telescope. An all-reflecting model using two mirrors has been designed and fabricated and used in the composite simulation (ref. 4). The principle of operation is illustrated in figure 10. In the top illustration, rays from the telescope optics are shown imaged on the focal plane after reflecting from two plane parallel mirrors. In operation the telescope will move, thereby causing all star images to move on the focal plane. The two mirrors are then rotated to bring the star images back to their original position. The two mirrors must be maintained parallel to each other as they are rotated. By doing this, all the stars within the field of view will be imaged on a plane that is parallel to the focal plane, but they will be changed in focus. This change in focus is eliminated if the path length from the top mirror to the focal plane is kept constant. This is accomplished by translating the bottom mirror along a parabola as it is rotated as shown in the bottom illustration of figure 10. Both mirrors have been rotated through the same angle, and the image has been translated along the focal plane. The distance between the two mirrors has changed, but the total path length remains constant.

The hardware for the compensator is shown in figure 11. The top view shows the complete assembly, whereas the bottom views show the mirror and the base assemblies.

Error Scaling Technique

To point the simulator to the required accuracy of 0.01 to 0.005 arc sec would require an extremely stable mechanical arrangement, very long optical paths, and probably would require the simulation to run in a vacuum. To circumvent these requirements, the error scaling technique of reference 5 was used. This error scaling technique can best be described by referring to the block diagram in figure 5. The scaling technique represented by the block diagram in figure 12 is similar to the control system shown in figure 5 except in this case the vehicle moment of inertia has been reduced by a factor K. The scale

factor K is used to reduce the moment of inertia of the large telescope to a value that can be easily simulated in the laboratory. For this simulation, K equals 5000, thereby reducing the pitch-axis moment of inertia I_V from 204 000 kg-m^2 (150 000 slug-ft^2) to 40.7 kg-m^2 (30 slug-ft^2). The disturbance torque T_d is shown to be reduced by a factor of $\sqrt{K}$; this increases the vehicle rate and attitude by a factor of $\sqrt{K}$, or in this case, a factor of 70.7. The momentum storage capability of the control moment gyro is reduced by a factor of $\sqrt{K}$ to compensate for the reduced disturbance torque. The sensor gain is reduced by a factor of $\sqrt{K}$ by changing the focal length of the sensor optics so that the image size and motion for the scaled system is the same as that for the unscaled telescope. The change in sensor gain compensates for the increase by a factor of $\sqrt{K}$ in vehicle attitude. Then all the inputs to the control moment gyro are rendered unscaled, and actual hardware may be used in the simulation with the sensor and angular momentum changes. The dynamic response of the scaled and unscaled control systems is identical.

Optical Scaling

The vehicle attitude in the coarse system has been scaled up by a factor of $\sqrt{K}$. The fine control system must therefore be scaled to insure that the image size and motion for the scaled errors are the same as those in the 3-meter telescope for unscaled errors. This is accomplished by using the optical scaling configuration shown in figure 13. This configuration was calibrated to give the correct image size and motion.

RESULTS AND DISCUSSION

The results of runs made with this simulation are divided into two main groups: Those run with the fine system pointing to a 107-μm (0.0042-in.) star image, the nominal diameter star image; and those where the system is pointing to a larger diameter, 188-μm (0.00741-in.) star image. The larger diameter star image runs were made to represent degradation in the image quality.

With the 107-μm-diameter star image, runs were made with +13.35, +12.3, and +11.25 magnitude stars. With the 188-μm-diameter star image, runs were made with +13.0, +12.3, and +11.35 magnitude stars. With the faintest star in each group the runs made were as follows: (a) Response to a step torque; (b) response to a torque pulse when the control moment gyro is driven by electrical signals onto the gyro gimbals when the range of the fine controller is near its limits; (c) acquisition, in which the fine system is turned on, acquires and locks onto the object star; (d) with the coarse system being driven sinusoidally at 3.08 scaled μrad (0.636 arc sec) peak to peak at 0.1 Hz; (e) with the coarse system being driven sinusoidally at 3.08 μrad (0.636 arc sec) peak to peak at 0.05 Hz; and (f) with the coarse system being driven sinusoidally at 3.08 μrad (0.636 arc sec) peak to peak at

0.025 Hz. For the next two faintest magnitudes the same runs were repeated except that the acquisition and pulsing runs were omitted.

Figure 14 shows the results of a scaled step torque of 0.00475 N-m (0.0035 ft-lb) applied to the coarse telescope. The fine control system is pointing to a +13.35 magnitude star with a 107-μm-diameter (0.0042-in.) star image. The scaled torque causes a steady-state scaled hangoff error of 3.42 μrad (0.707 arc sec) on the coarse system as shown labeled θ_v in figure 14. The angle of the IMC mirrors θ_m shown on the next trace indicates that the mirrors move in a similar manner to take up the error, thereby leaving virtually no indication of the step shown in the bottom trace.

Figure 15 shows the result of the fine-pointing sensor acquiring the same +13.35 magnitude star with a 107-μm-diameter (0.0042-in.) image. The trace θ_v shows the response of the vehicle to a steady torque. The next trace θ_m shows that the IMC mirrors, immediately after the system is turned on, acquire the star and assume a position such that θ_e remains at its nominal value. The trace labeled "field of view" indicates the operating field of view and shows that, once turned on, the system went immediately from the cage position, field of view 1, to field of view 5, the narrowest and most sensitive one. This transition happened so fast that it is barely visible on the trace.

Figure 16 shows the results of pulsing the control moment gyro with the fine system pointing to a +13.35 magnitude star with an image 107 μm in diameter. In this case the vehicle is pulsed by an electrical signal to the CMG gimbal, triggered when the digital computer monitors the mirror position θ_m and determines that it has reached a preset level. When this level is reached, the pulse is sent to the gimbal to drive the coarse vehicle toward zero error. The sawtooth seen on the trace is the result of the vehicle continuously being driven such that the mirrors reach that predetermined level.

Figure 17 shows the results obtained when the coarse system is driven by a sinusoidal input to the CMG gimbal of 0.1 Hz at an amplitude sufficient to drive the coarse system to 0.636 arc sec peak to peak. In this run the fine system is pointing to a +13.35 magnitude star with an image 107 μm (0.0042 in.) in diameter. Runs of this type were made for three different star magnitudes with an image diameter of 107 μm (0.0042 in.) and for three more star magnitudes with an image diameter of 188 μm (0.00741 in.). A listing of these runs is given in table 1.

Photographic film records were made for each of the runs with the sinusoidal input to the coarse system. Records were made by using another star source through the same control system optics and directed to a film drum rather than the fine sensor. The film drum had a circumference of 0.33 m (13 in.) and made one revolution in 105 seconds. The shaft was threaded with 4409 threads per m (112 threads per in.), giving a translation of 227 μm (0.0089 in.) per revolution. The average time duration of each run was 18 minutes. A segment of the film for each simulation run is presented in figures 18 to 23. A

typical segment will show 10 traces with each trace representing approximately 2 seconds of each run. Each trace is separated in time by 105 seconds.

Figure 18 shows the results obtained with the fine system pointing to +13.35 magnitude star with an image diameter of 107 μm (0.0042 in.) while the coarse system or telescope body is being driven at 0.636-arc-sec amplitude peak to peak at 0.1, 0.05, and 0.025 Hz.

Figure 19 shows the results of pointing to a +13.0 magnitude star with an image 188 μm in diameter with the coarse system being driven at 0.636-arc-sec magnitude peak to peak at 0.1, 0.05, and 0.025 Hz. Figures 20 and 21 show the results of pointing to a +12.3 magnitude star with image diameters of 107 μm and 188 μm, respectively, at 0.1, 0.05, and 0.025 Hz. Figure 22 shows results of using an +11.25 magnitude star with an image 107 μm in diameter at 0.1, 0.05, and 0.025 Hz, and figure 23 shows an +11.35 magnitude star with an image diameter of 188 μm at 0.1, 0.05, and 0.025 Hz. The magnitude of the disturbance in all cases was 0.636 arc sec peak to peak.

Table 1 gives a value for the standard deviation for each of the runs in image diameters and arc seconds. These values were determined by reading the film lines on a film reader and comparing where the line is and where it should be at several points along the film strip. From these data points the standard deviation was computed. To test the accuracy of the readout using this method, the same data points on the same film were read out twice and the difference in corresponding readings was determined. The root-mean-square error between the two readings was 0.05 image diameter, the equivalent of 0.00359 scaled arc sec. This error is significant for this type of readout and in this case represents one-half the accuracy set as the goal for the fine-pointing control system, which is one-tenth of an image diameter. Consequently, interpolation of the numerical data in table 1 must take this reading accuracy into account. For this reason, photographs of the actual film traces in figures 18 to 23 have been included so that a more graphic illustration of errors can be given.

CONCLUDING REMARKS

The laboratory simulation of a scaled single-axis dual-level pointing control system has been demonstrated. The results of the simulation indicate that the body-pointing requirements of a large space telescope can be relaxed to a relatively coarse accuracy while maintaining image position control on the focal plane of the telescope with the use of a secondary level control system. The results further indicate that the fine control system presented here can be used to stabilize the star image of a 3-meter diffraction-limited telescope to within one-tenth of an image diameter for stars as dim as +12.3 visual magnitude while the vehicle is subjected to nominal disturbance torques. The results also show

that the system can be used to stabilize stars as dim as +13.35 visual magnitude with somewhat reduced accuracy. The simulation also demonstrated the application of the error scaling technique to the laboratory simulation of precision pointing systems.

Langley Research Center
National Aeronautics and Space Administration,
Hampton, Va., July 6, 1973.

REFERENCES

1. Anon.: A System Study of a Manned Orbital Telescope. D2-84042-1 (Contract NAS 1-3968). Boeing Co., Oct. 1965. (Available as NASA CR-66047.)

2. Ostroff, Aaron Joel.: Design of a Star Image Regulating System Utilizing a Digital Sensor. M.S. Thesis, George Washington Univ., Feb. 1971.

3. Ostroff, Aaron J.; and Romanczyk, K. C.: Design of an Electronically Scanned Star Sensor With Digital Output. NASA TN D-5281, 1969.

4. Romanczyk, K. C.; Ostroff, Aaron J.; and Howell, W. E.: Design and Analysis of a Star Image Motion Compensator. NASA TN D-7145, 1973.

5. Bullock, Gordon F.; and Morrell, Frederick R.: A Scaling Technique for an Air-Bearing Simulation of Precision Systems. NASA TN D-6197, 1971.

6. Ostroff, Aaron J.; and Romanczyk, K. C.: Design and Evaluation of an Optical Fine-Pointing Control System for Telescopes Utilizing a Digital Star Sensor. NASA TN D-7204, 1973.

TABLE 1.- PARAMETERS AND RESULTS FOR PHOTOGRAPHIC FILM RECORDS

Figure	Star visual magnitude	Star image diameter, μm	Disturbance torque magnitude, arc sec	Disturbance torque frequency, Hz	Standard deviation, nominal image diameters	Standard deviation, arc sec
18(a)	13.35	107	0.636	0.1	0.157	0.0114
18(b)	13.35	107	.636	.05	.158	.0114
18(c)	13.35	107	.636	.025	.117	.0084
20(a)	12.3	107	.636	.1	.0814	.0058
20(b)	12.3	107	.636	.05	.095	.00686
20(c)	12.3	107	.636	.025	.095	.00686
22(a)	11.25	107	.636	.1	.0606	.00437
22(b)	11.25	107	.636	.05	.0610	.0044
22(c)	11.25	107	.636	.025	.0545	.00392
19(a)	13.0	188	.636	.1	.189	.0136
19(b)	13.0	188	.636	.05	.101	.0073
19(c)	13.0	188	.636	.025	.1106	.00835
21(a)	12.3	188	.636	.1	.140	.0105
21(b)	12.3	188	.636	.05	.0812	.00585
21(c)	12.3	188	.636	.025	.0845	.0061
23(a)	11.35	188	.636	.1	.0866	.00625
23(b)	11.35	188	.636	.05	.0867	.00626
23(c)	11.35	188	.636	.025	.0528	.0038

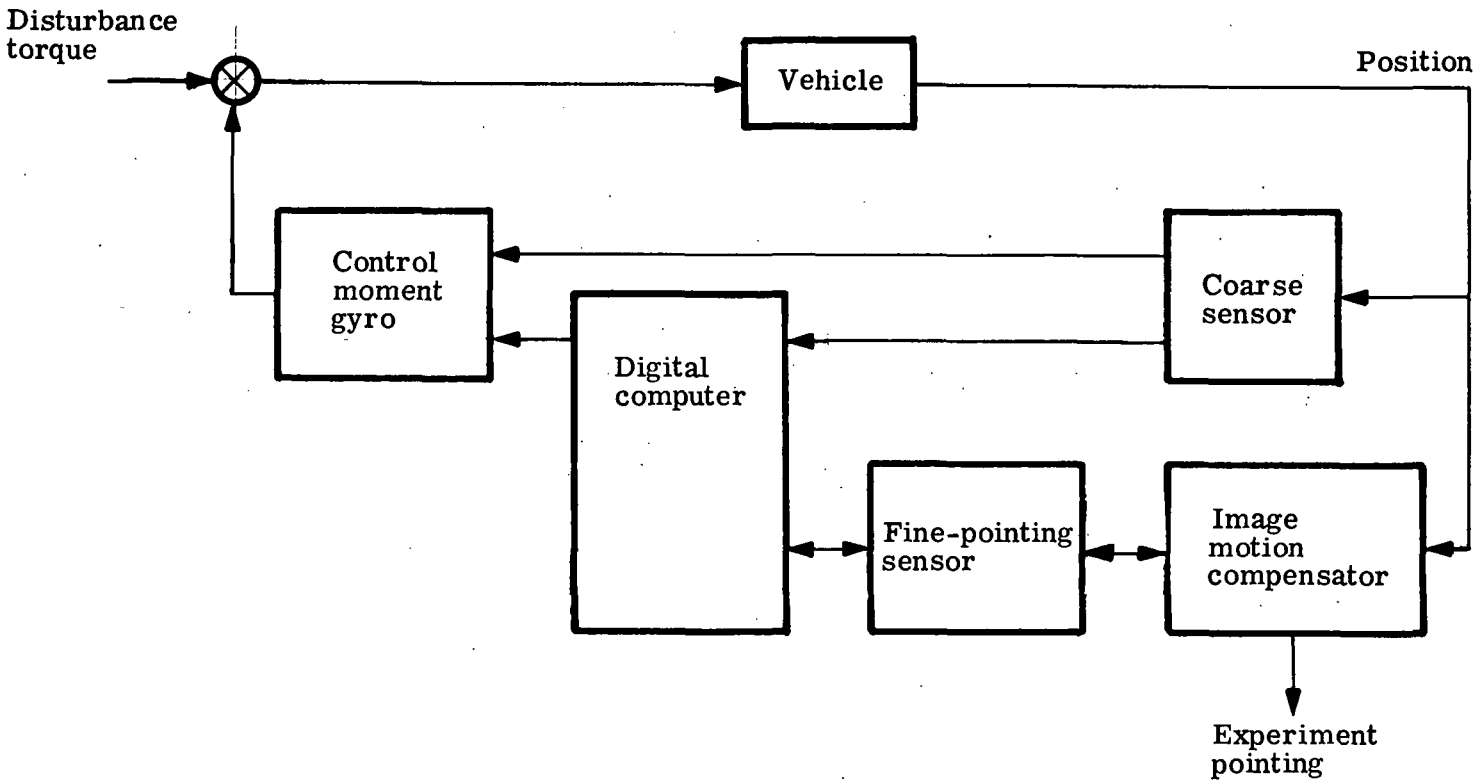

Figure 1.- Block diagram of dual-level control system.

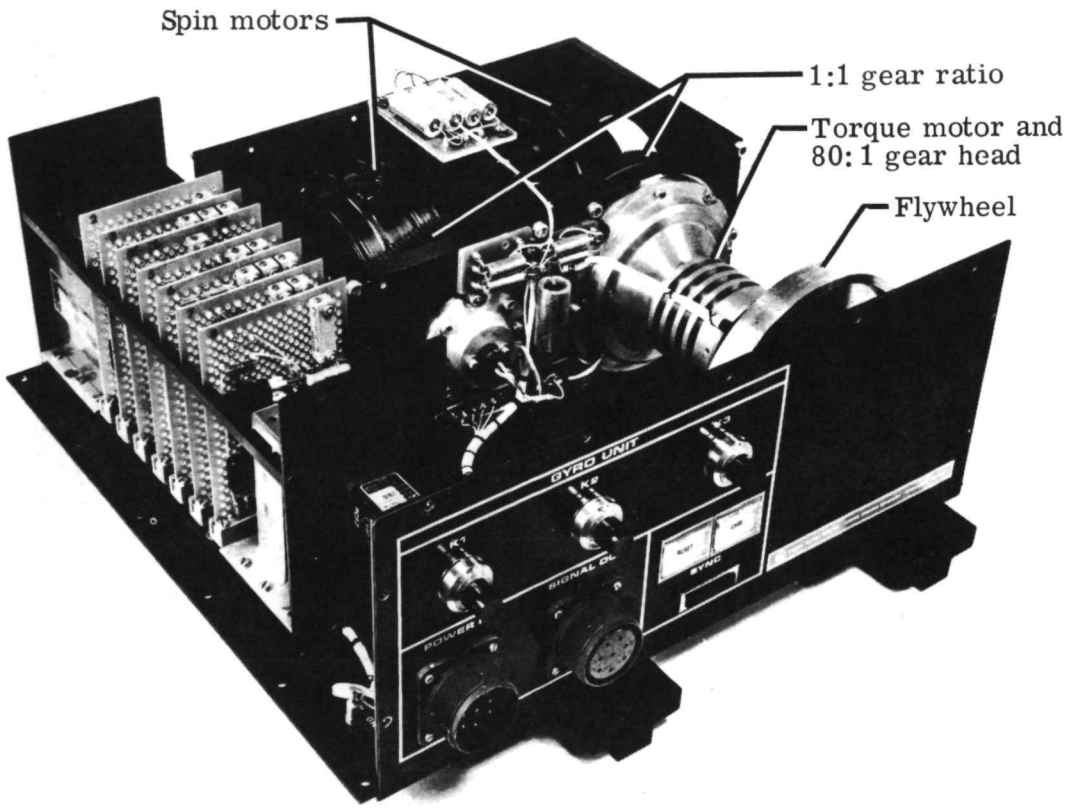

L-71-532

Figure 2.- Control moment gyro unit.

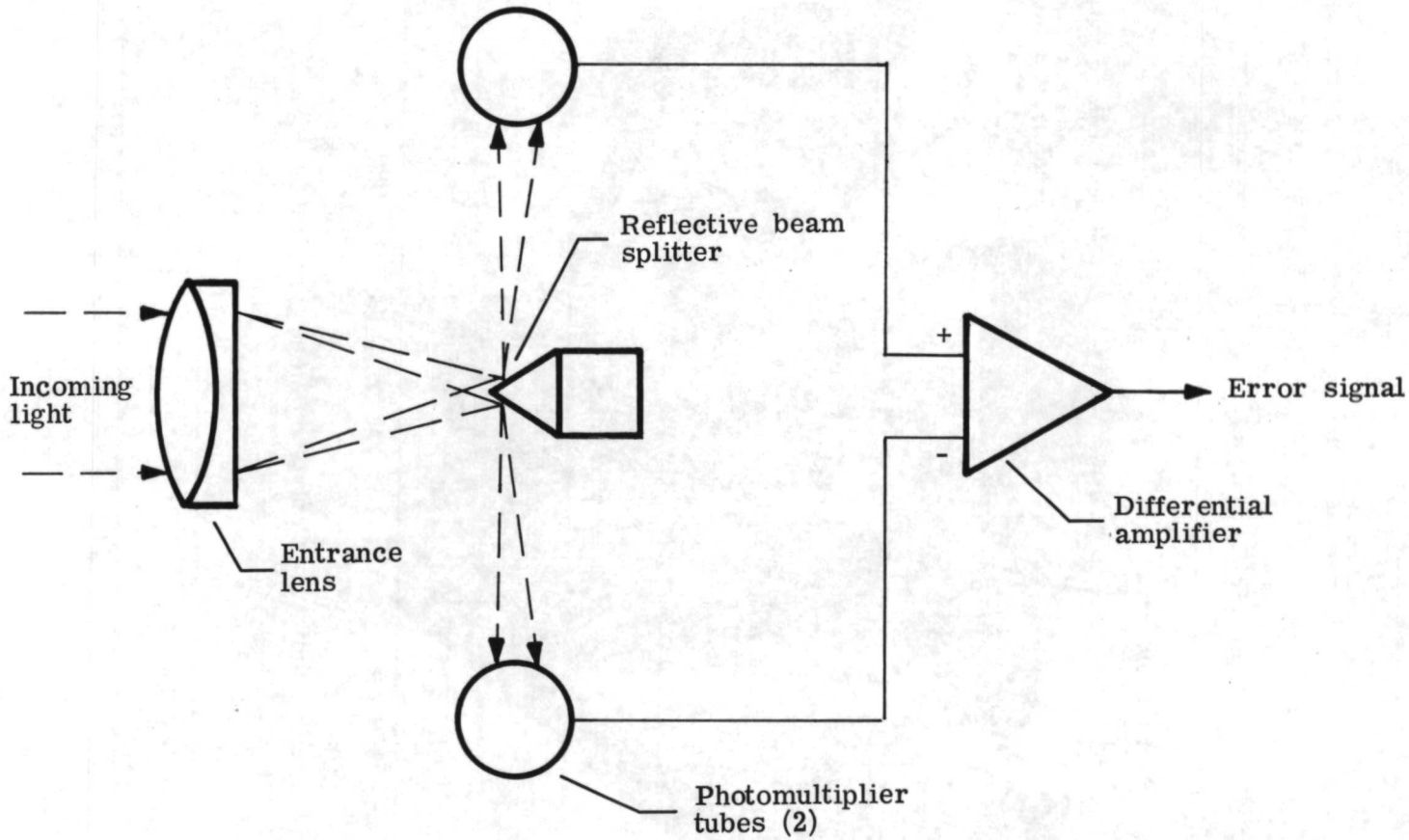

Figure 3.- Reflective beam-splitter-type star sensor for coarse-pointing system.

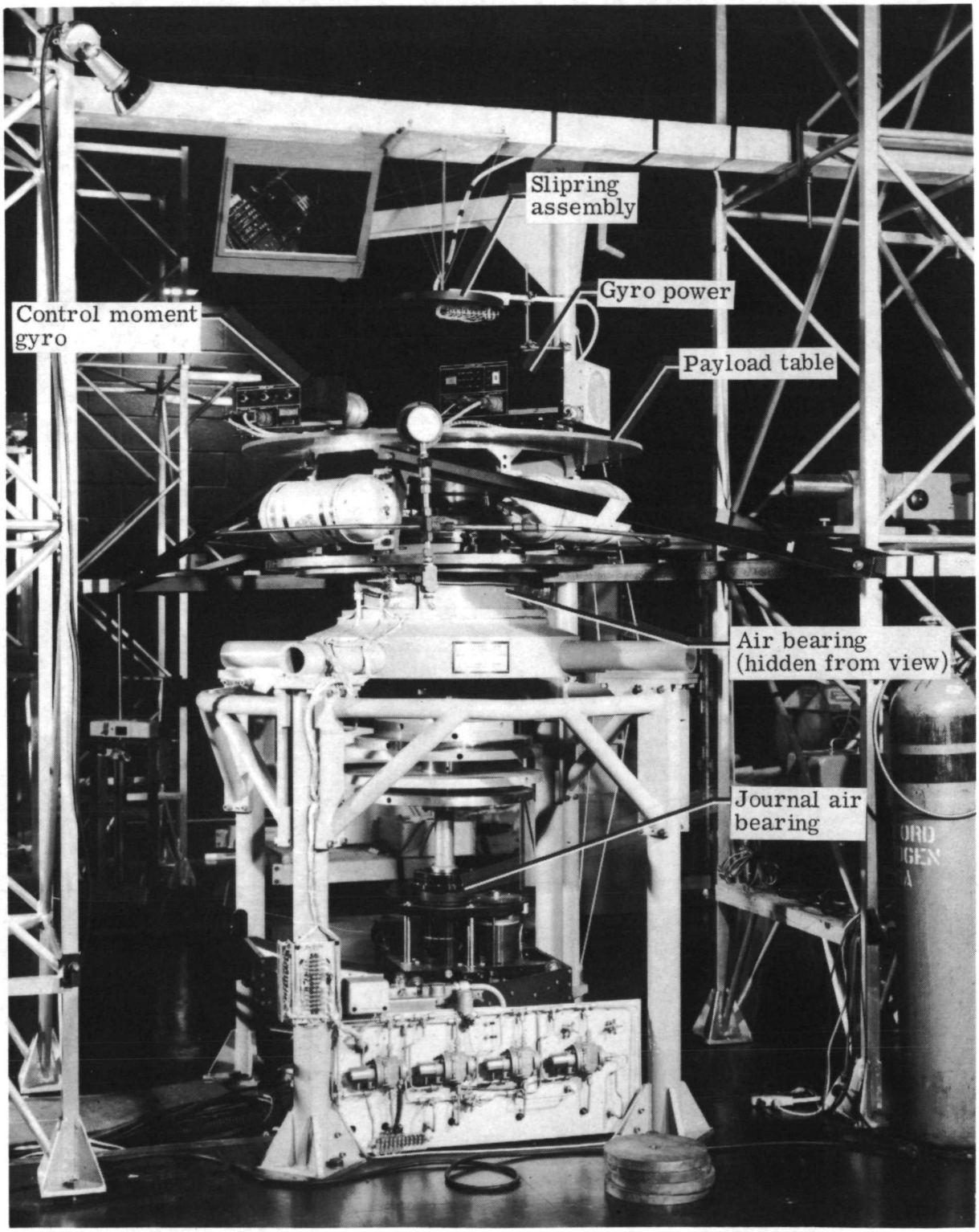

L-69-7007.1

Figure 4.- Vehicle inertia simulator and associated equipment.

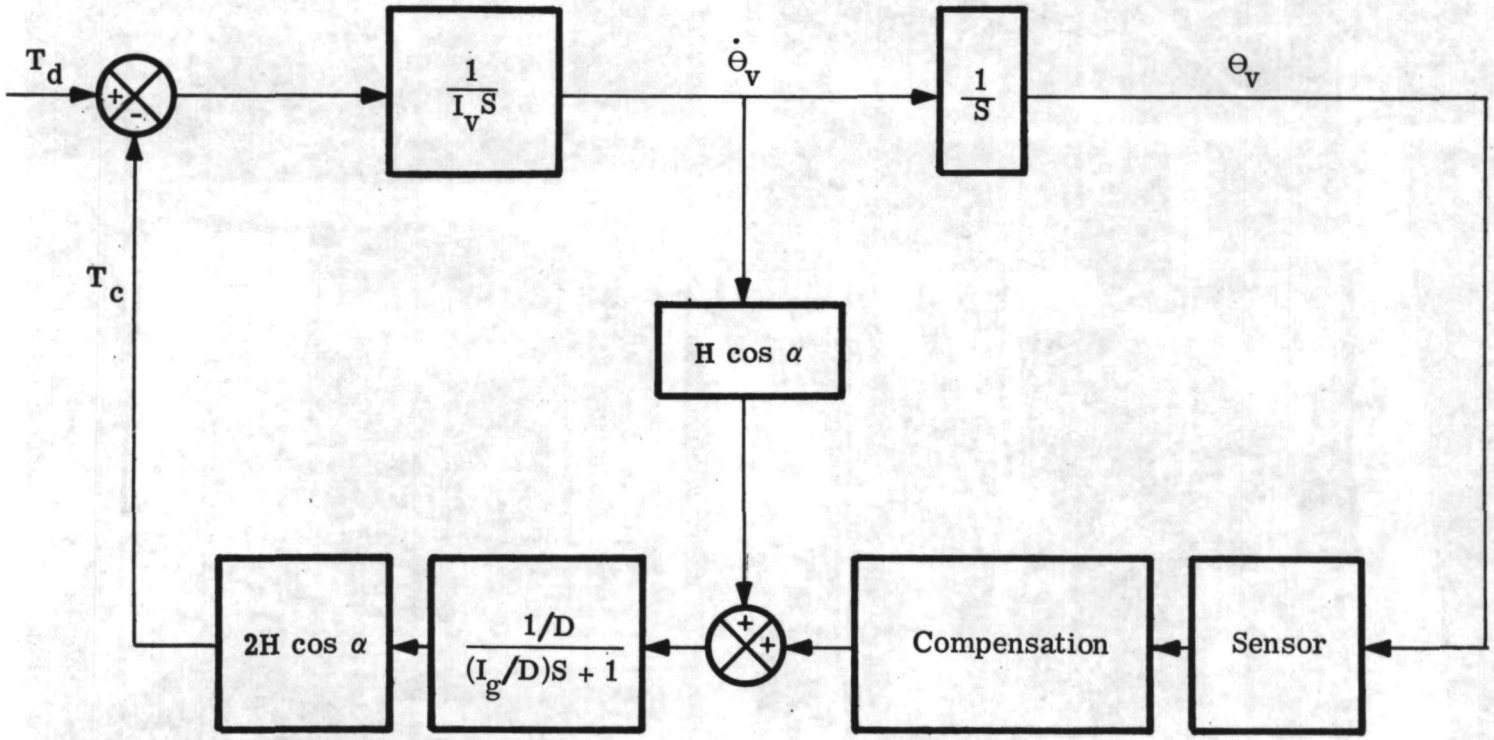

Figure 5.- Simplified block diagram of single-axis coarse-control system.

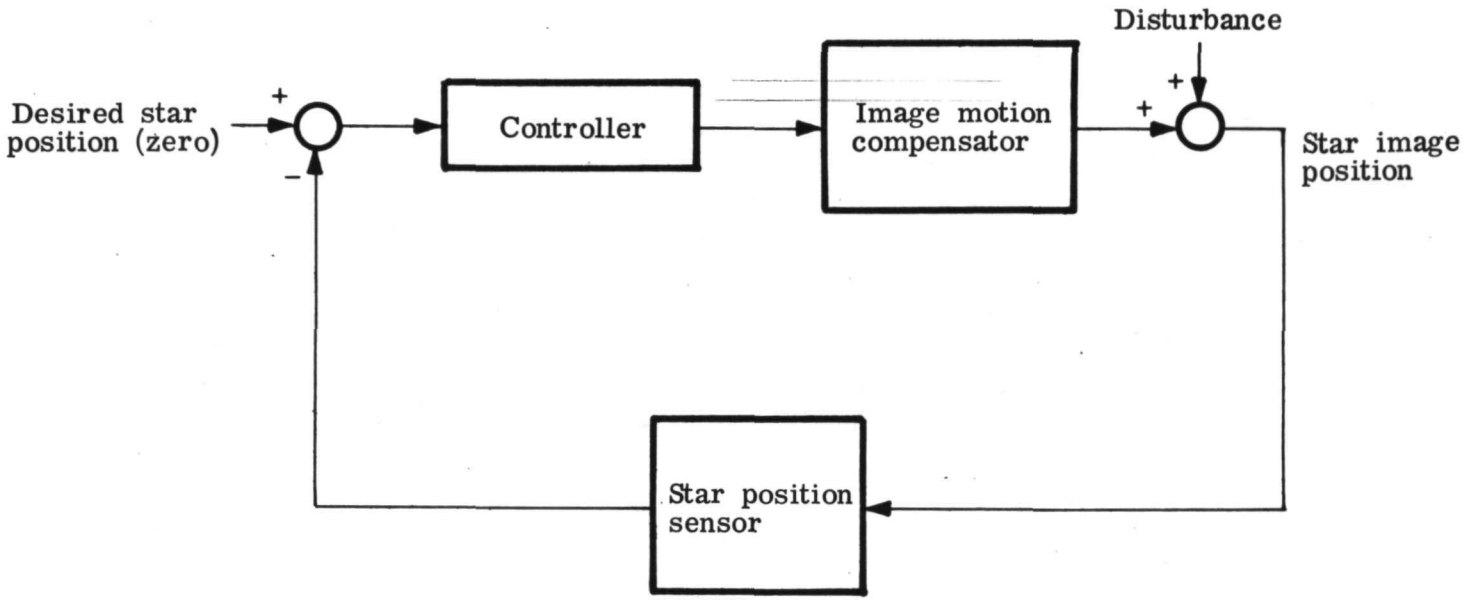

Figure 6.- Simplified block diagram of fine-pointing control system.

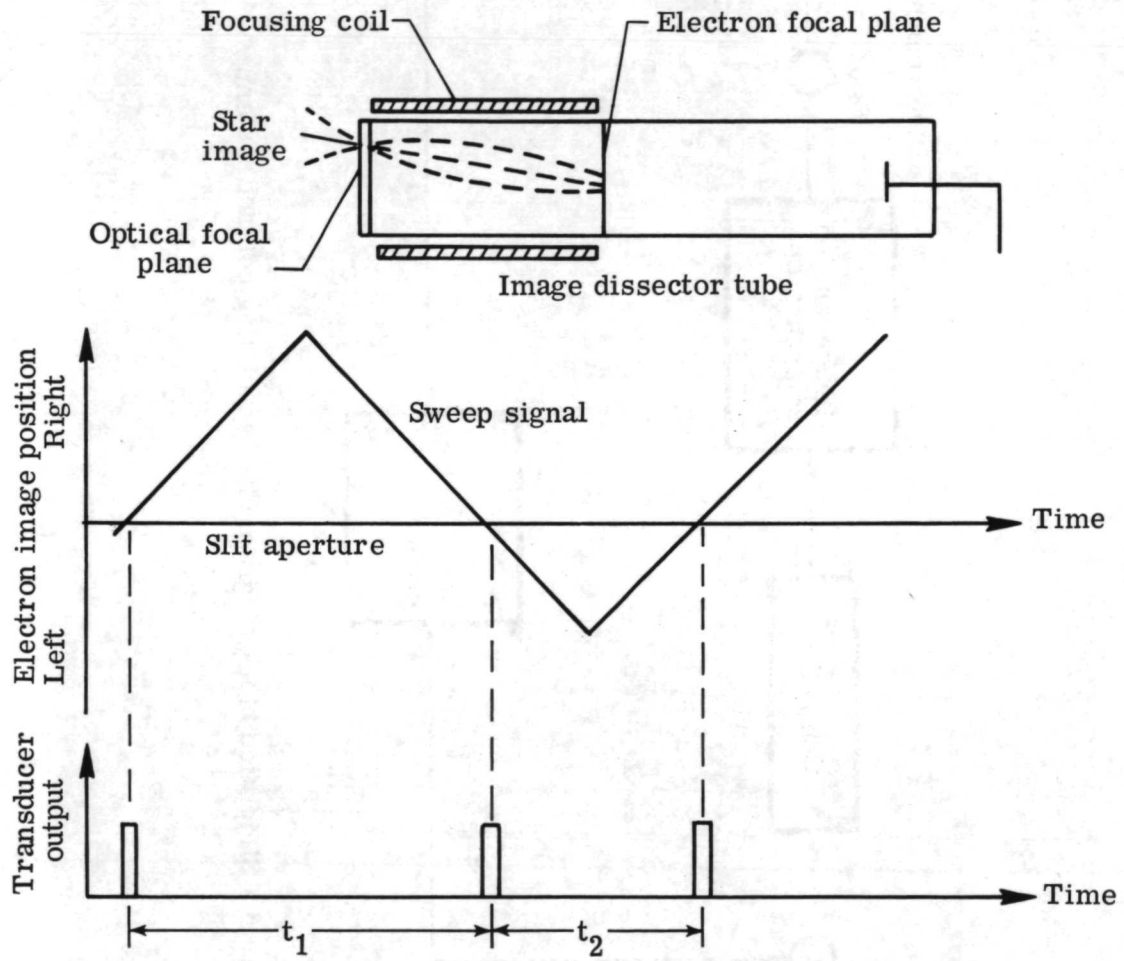

Figure 7.- Schematic representation of fine-pointing sensor, sweep signal, and output pulses.

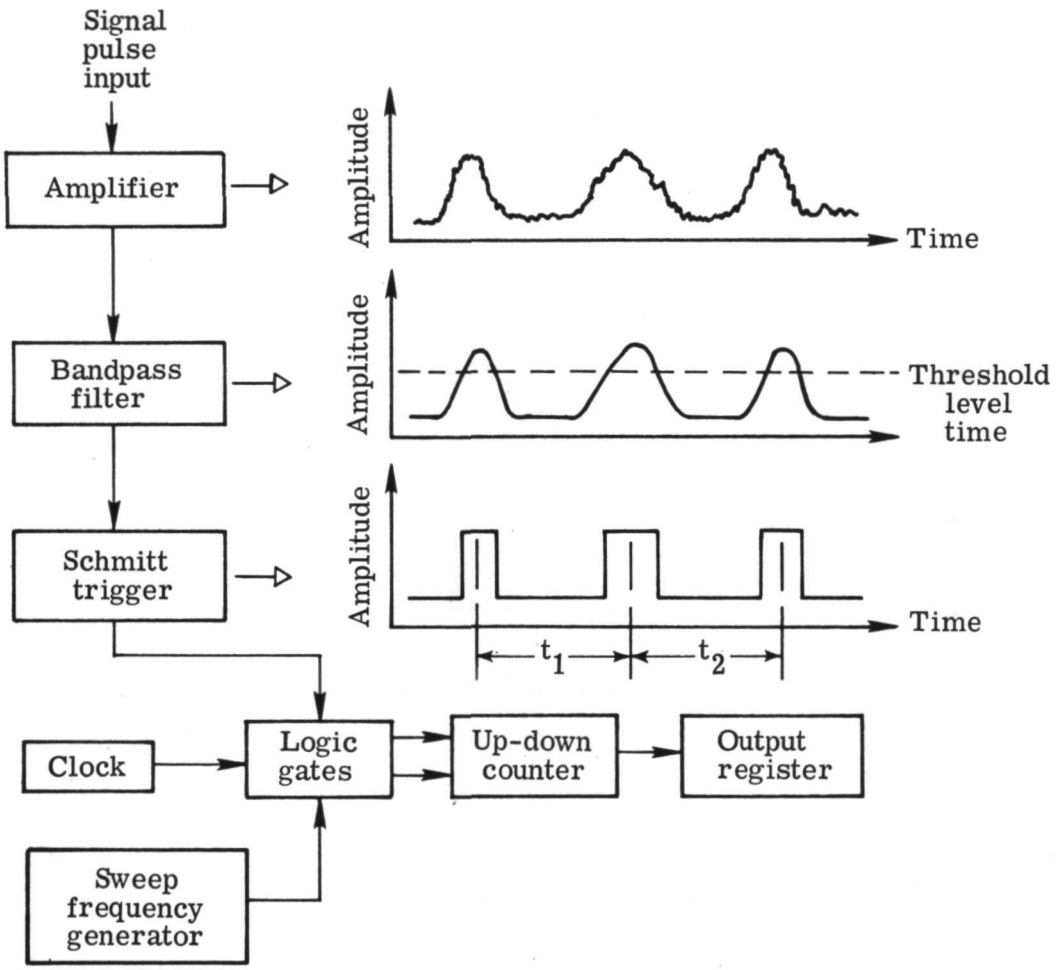

Figure 8.- Schematic representation and typical waveforms of signal processing system.

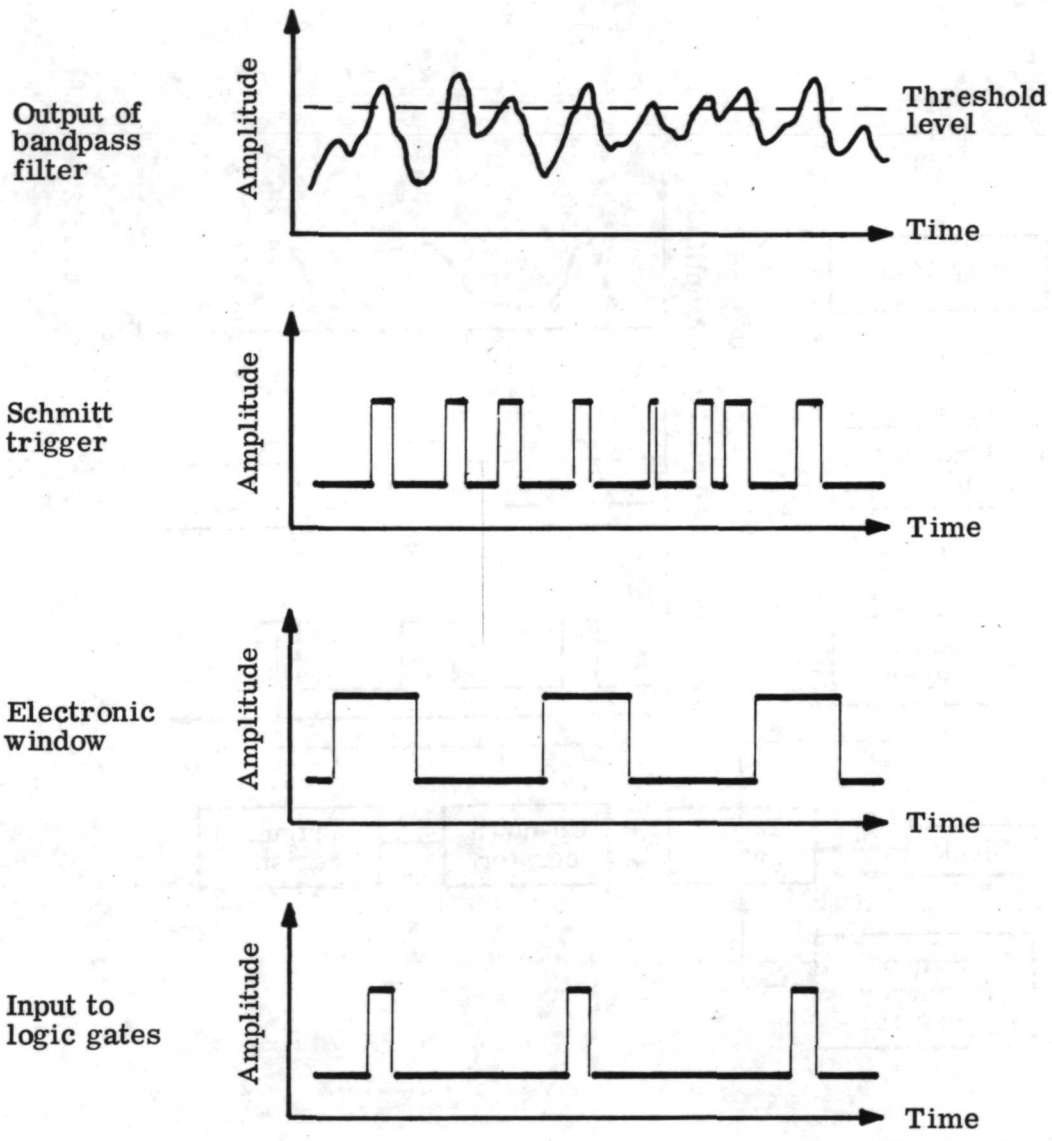

Figure 9.- Relationship of electronic window to pulse train.

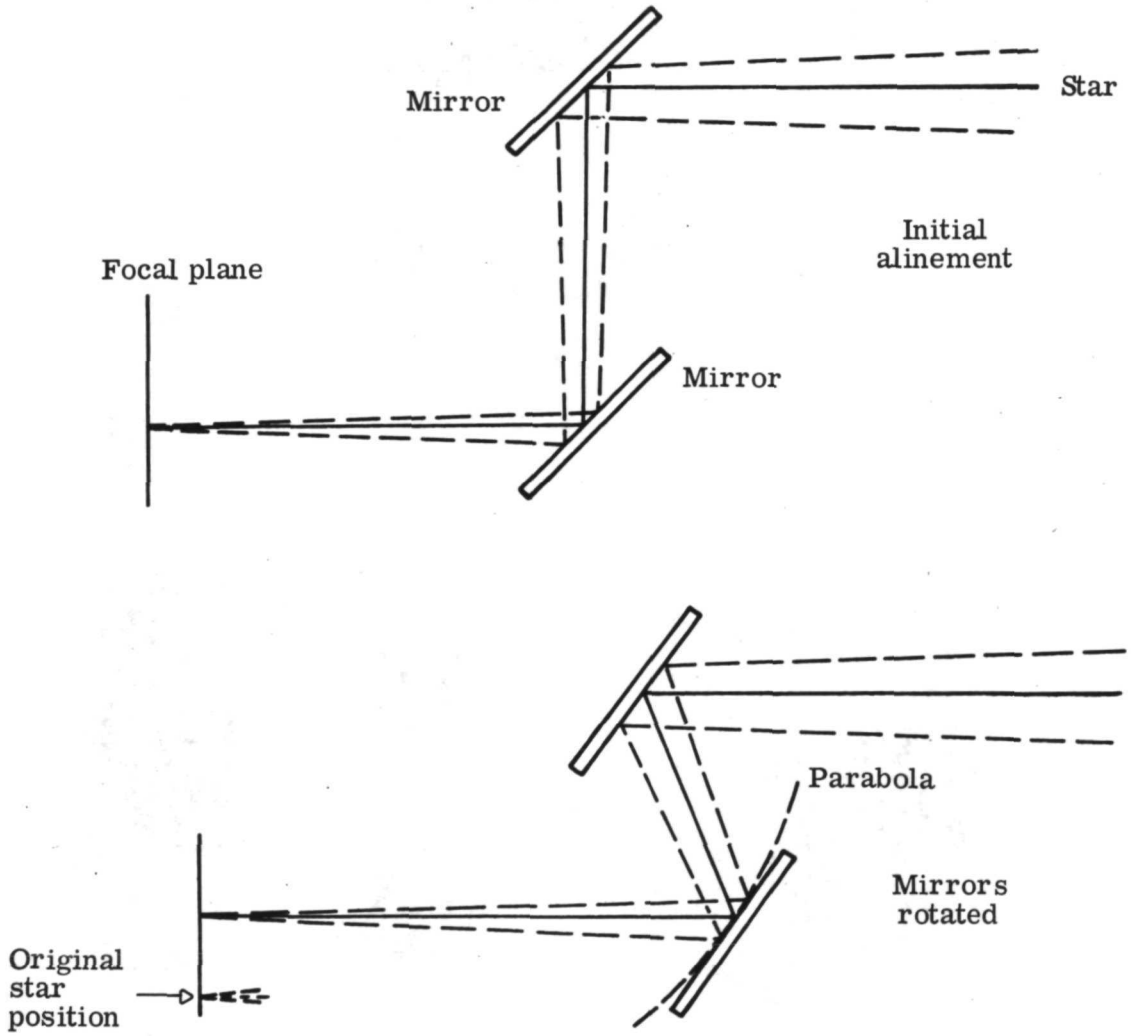

Figure 10.- Schematic representation of image motion compensator.

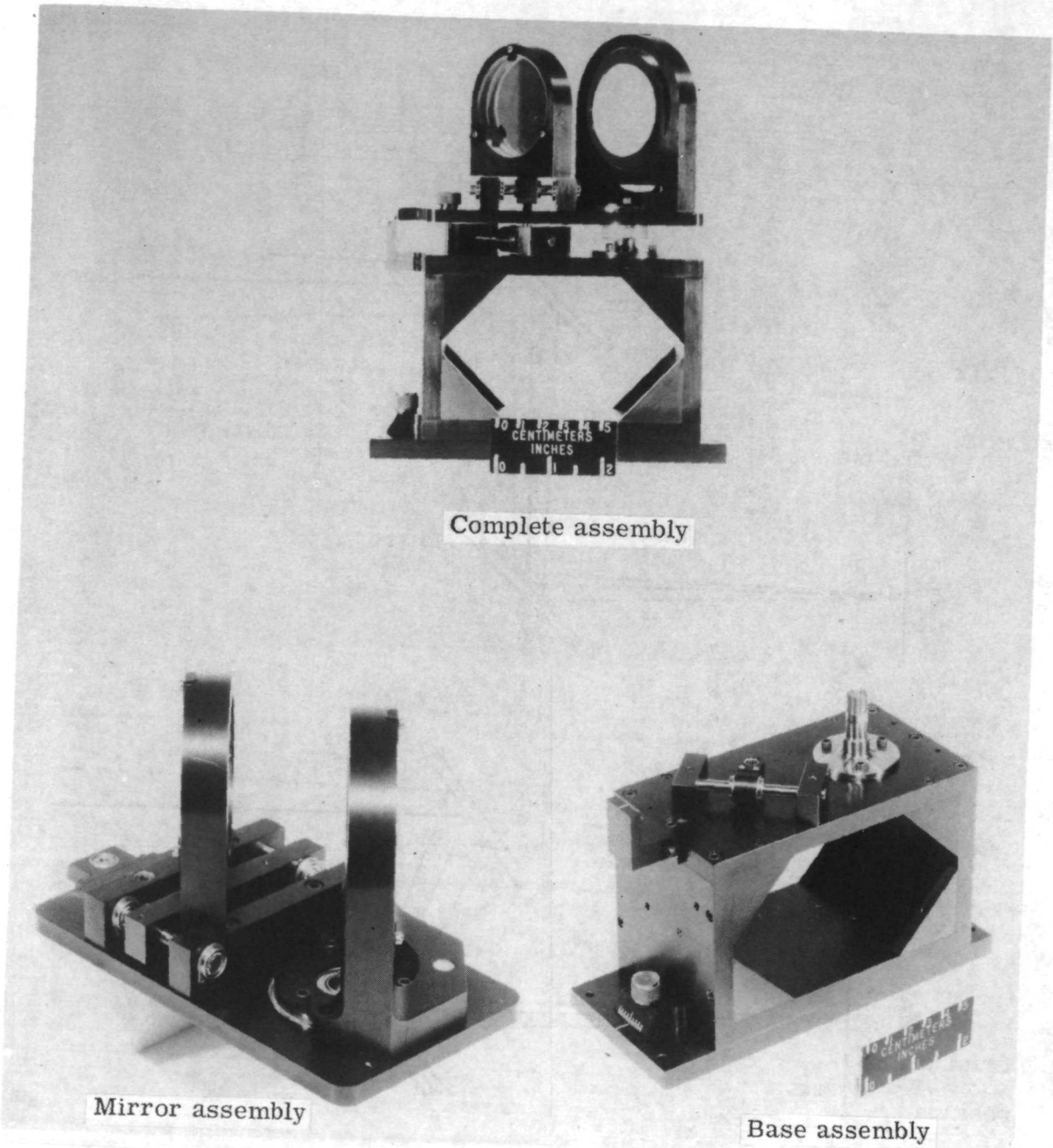

L-73-6804

Figure 11.- Image-motion-compensator hardware.

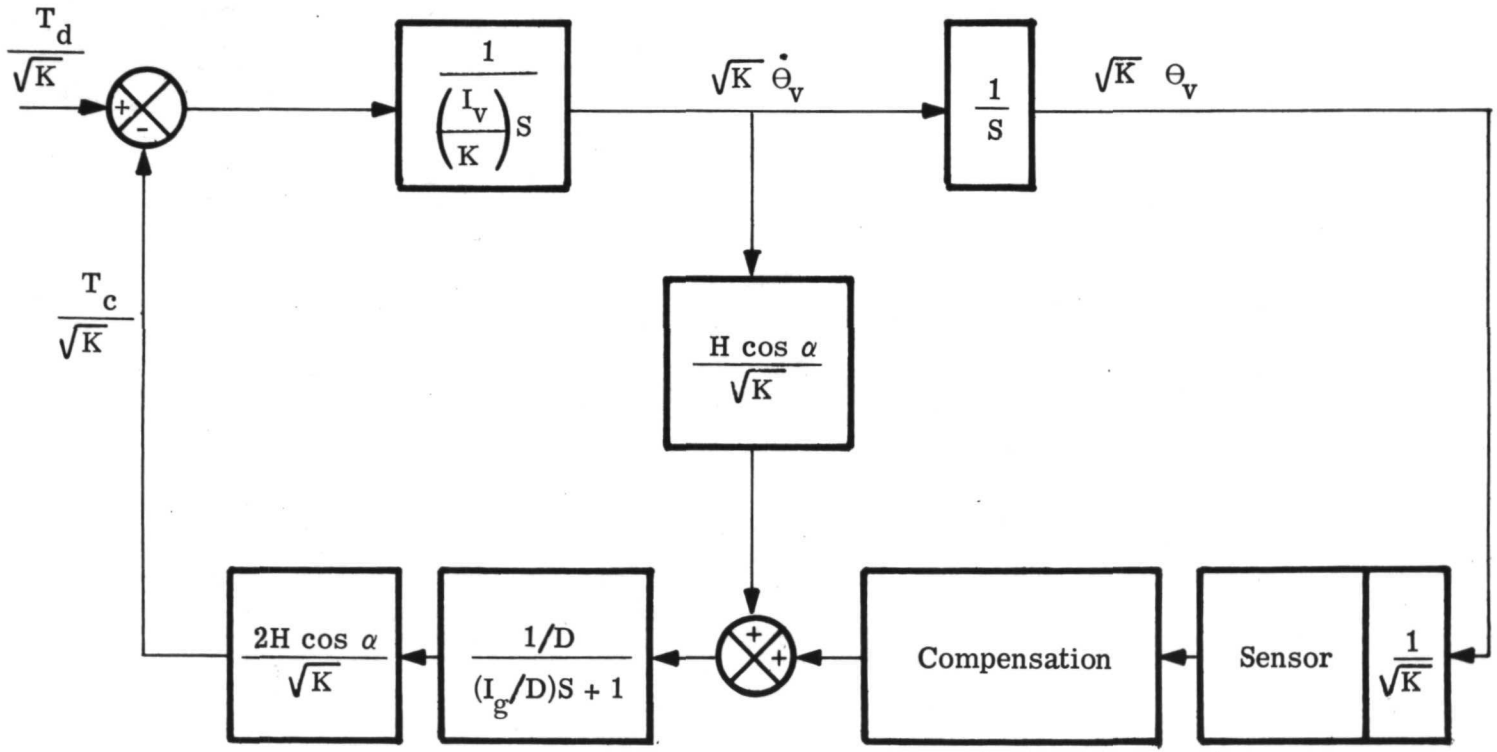

Figure 12.- Simplified block diagram of scaled single-axis coarse-control system.

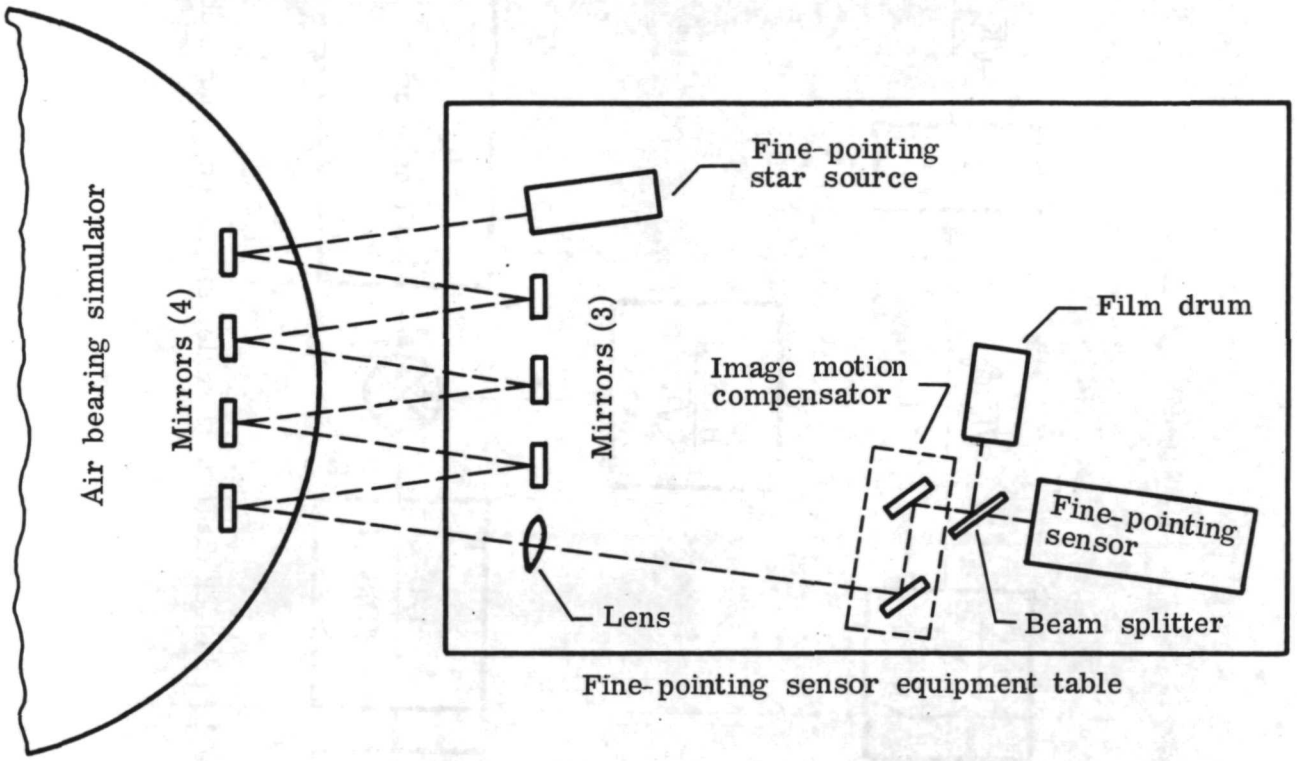

Figure 13.- Optical scaling diagram.

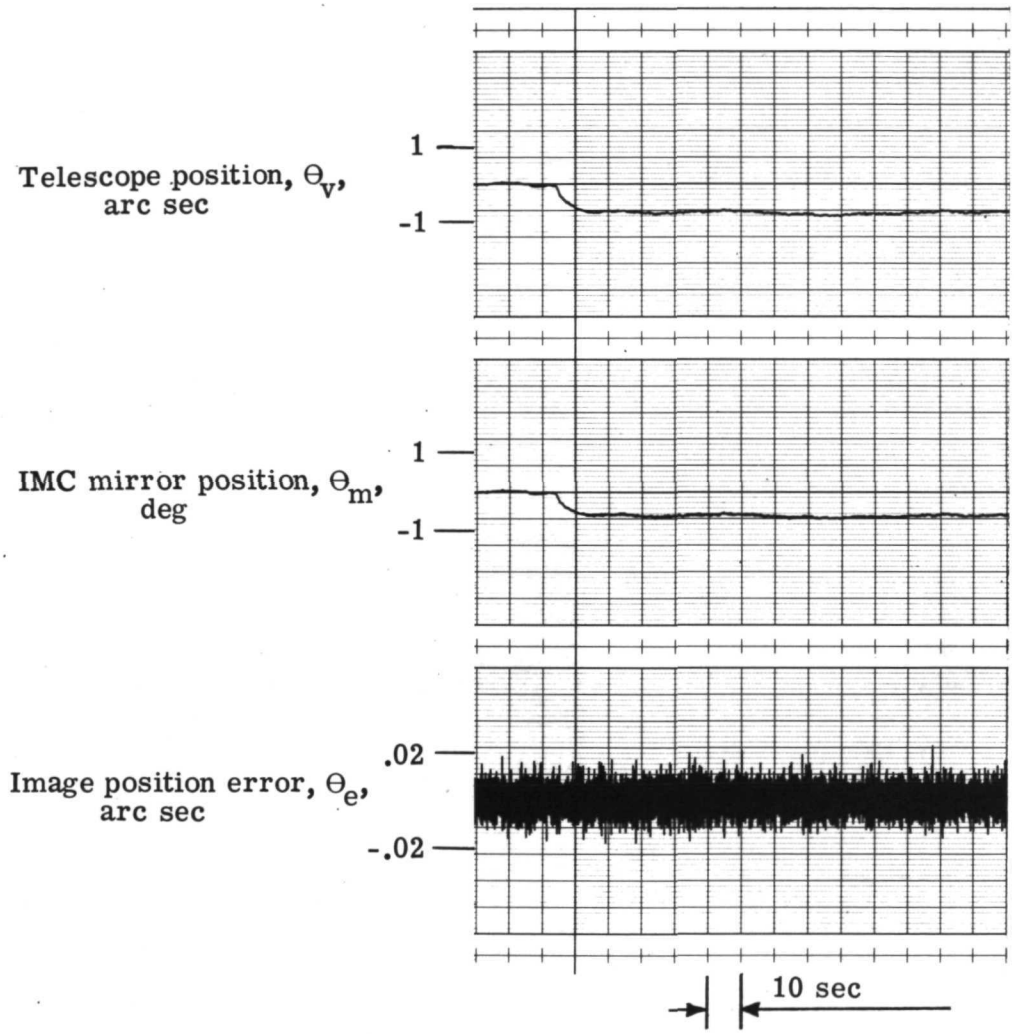

Figure 14.- Response to step torque with fine system pointing to +13.35 magnitude star with image diameter of 107 μm.

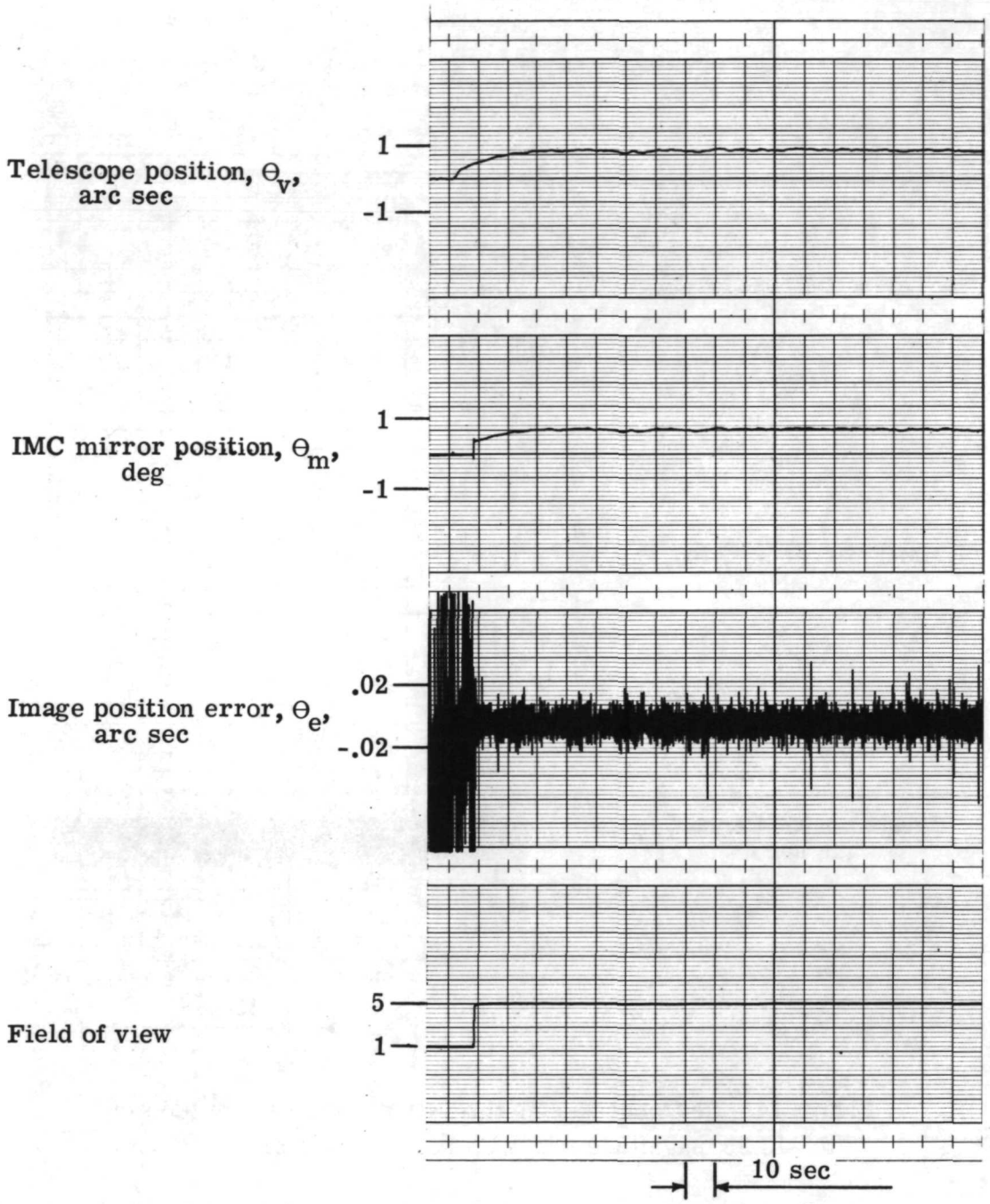

Figure 15.- Acquisition of +13.35 magnitude star with image diameter of 107 μm.

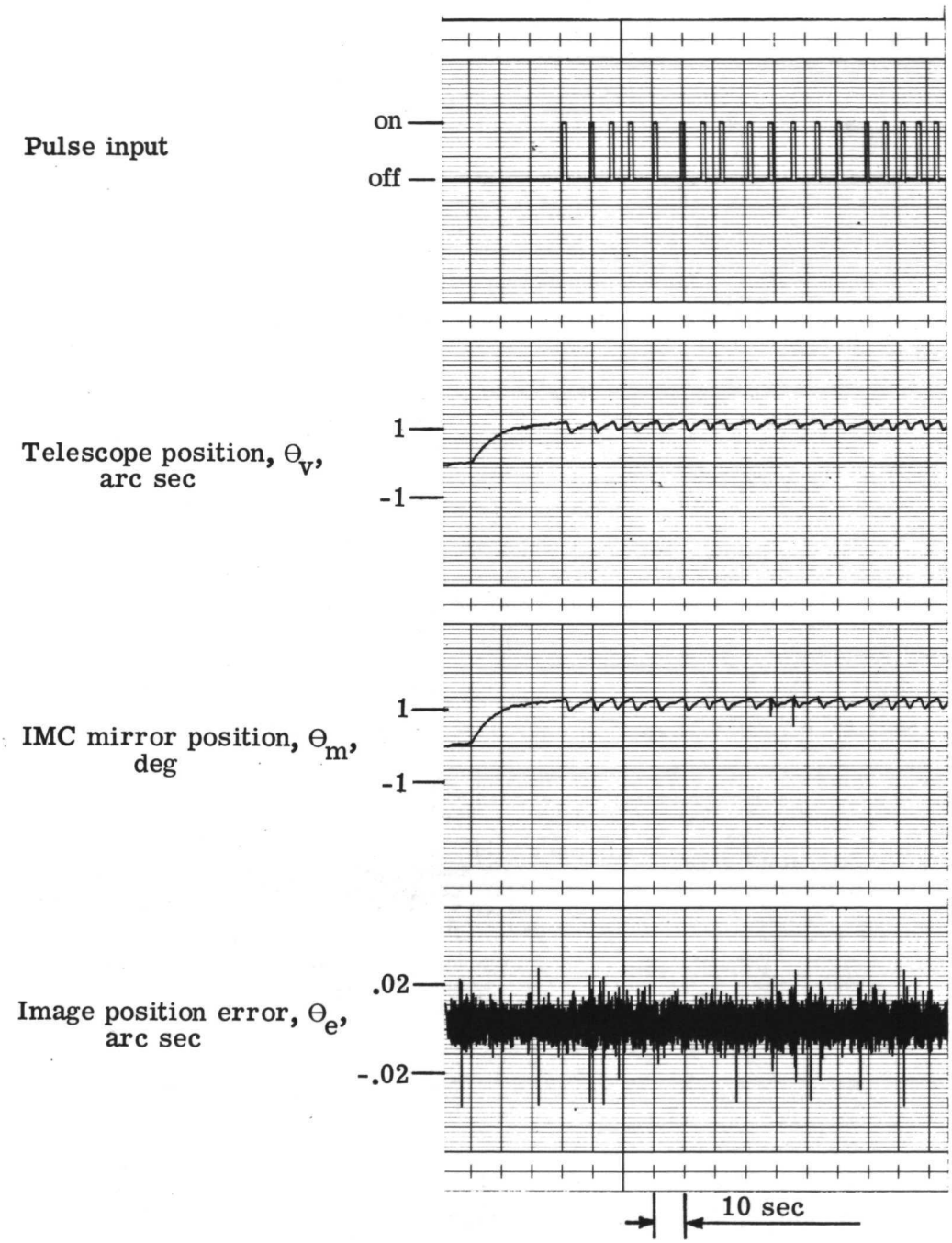

Figure 16.- Pulsing coarse-control system with fine system pointing to +13.35 magnitude star with image diameter of 107 μm.

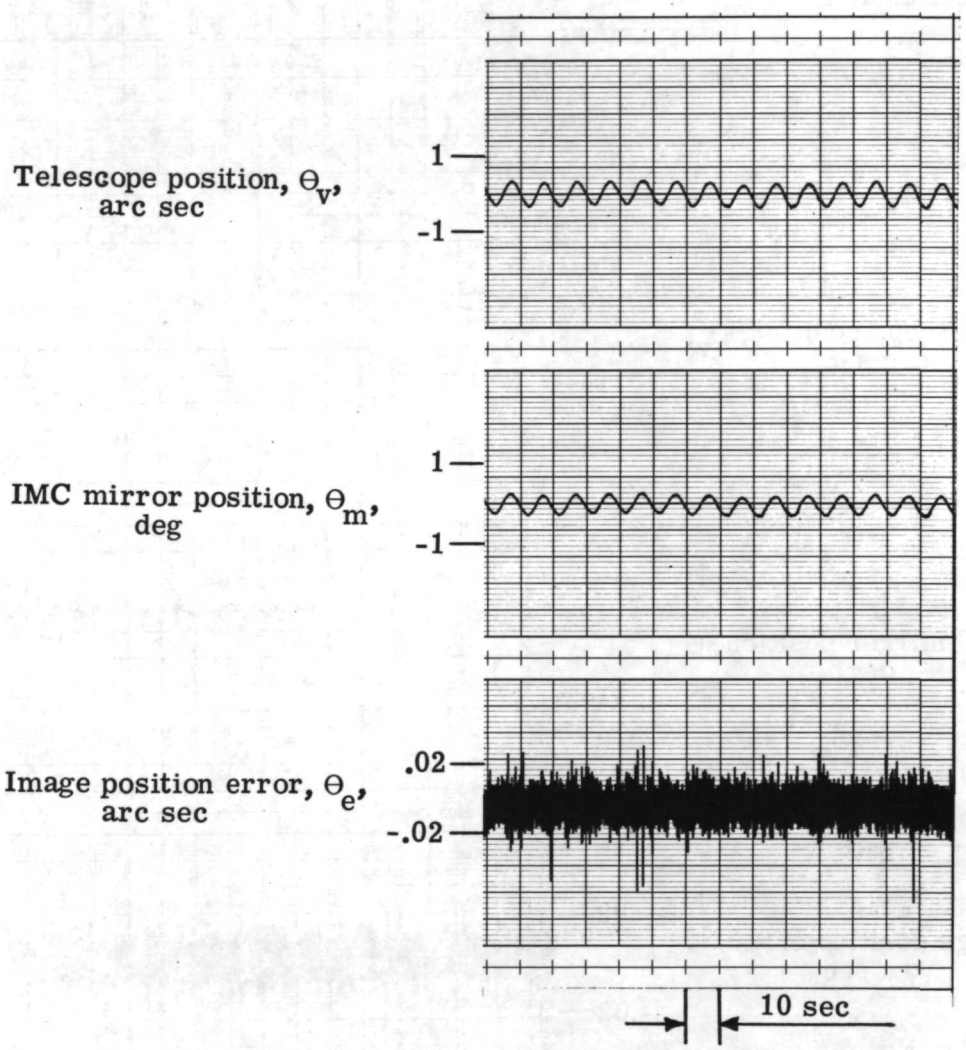

Figure 17.- Response of fine-pointing system to +13.35 magnitude star with image diameter of 107 μm with coarse system being driven sinusoidally to 0.636-arc-sec peak-to-peak amplitude at 0.1 Hz.

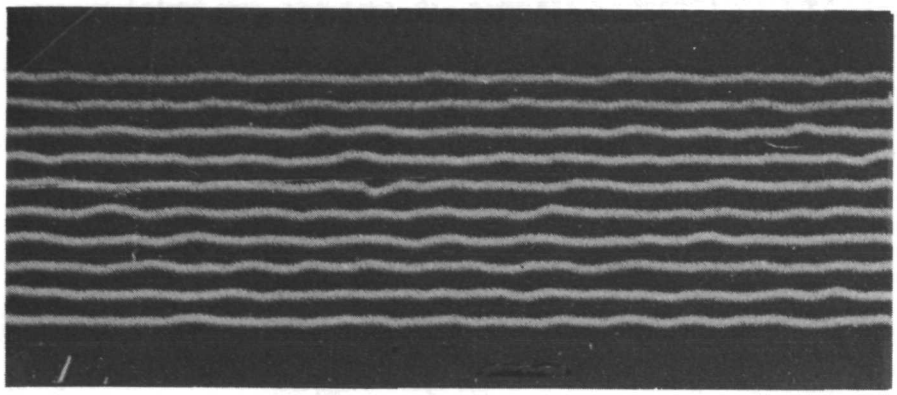

(a) 0.636 arc sec at 0.1 Hz.

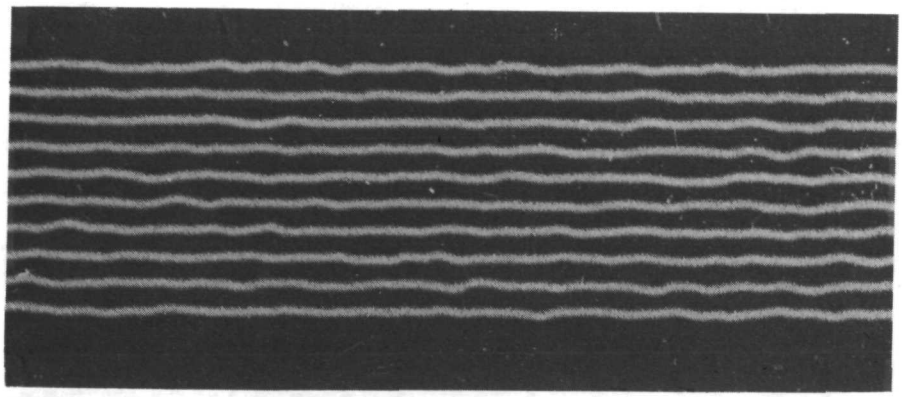

(b) 0.636 arc sec at 0.05 Hz.

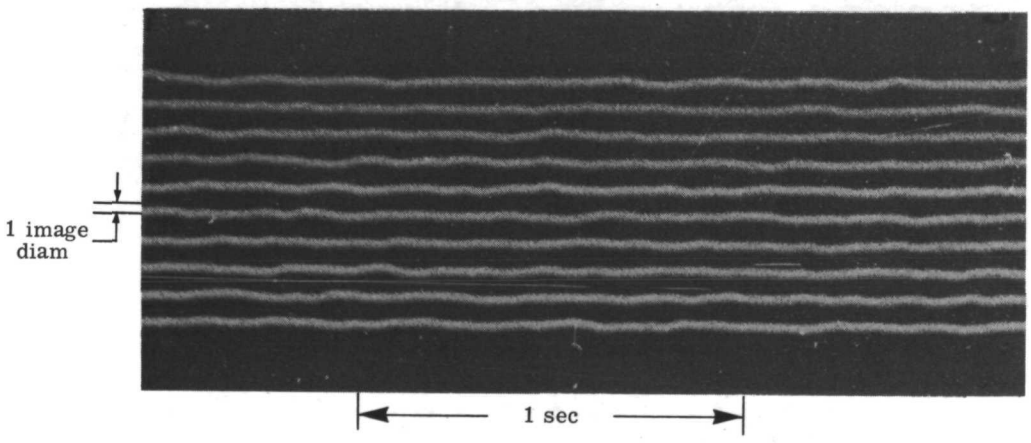

(c) 0.636 arc sec at 0.025 Hz. L-73-6805

Figure 18.- Image stability of fine control system to +13.35 magnitude star with image diameter of 107 μm when coarse system is being driven sinusoidally at indicated amplitude and frequency.

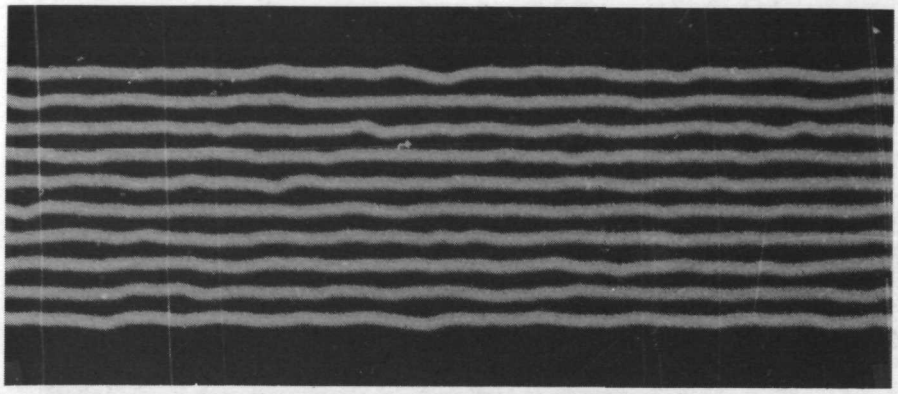

(a) 0.636 arc sec at 0.1 Hz.

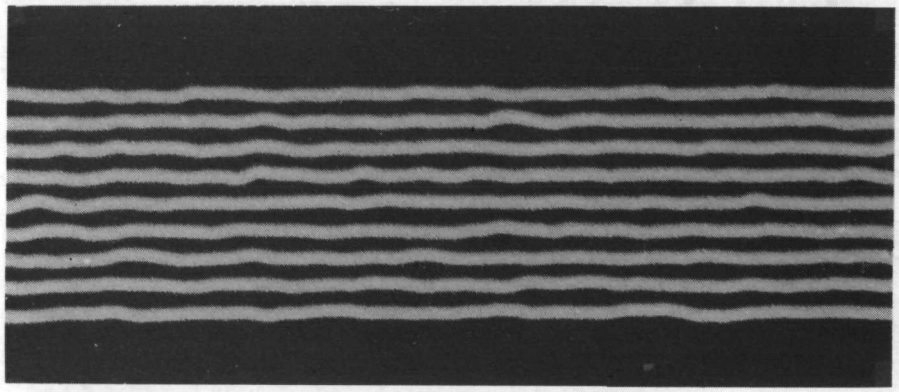

(b) 0.636 arc sec at 0.05 Hz.

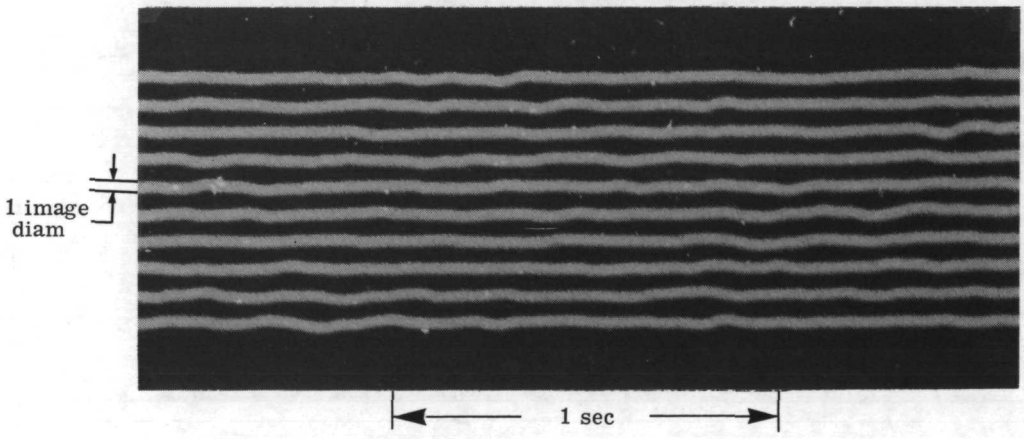

(c) 0.636 arc sec at 0.025 Hz. L-73-6806

Figure 19.- Image stability of fine system to +13.0 magnitude star with image diameter of 188 μm with coarse system being driven sinusoidally at indicated amplitude and frequency.

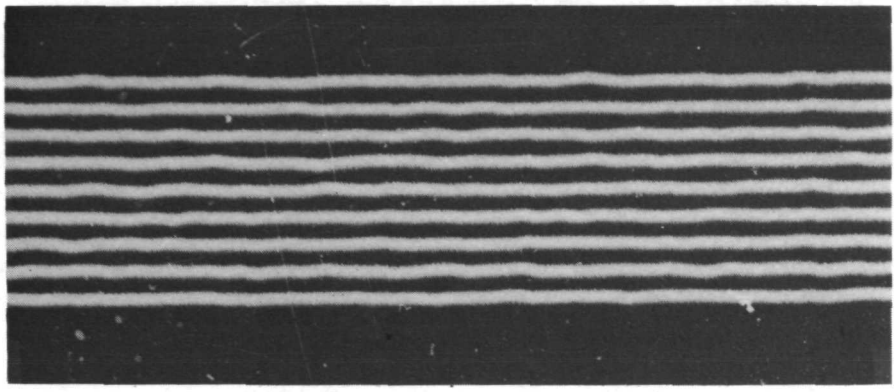

(a) 0.636 arc sec at 0.1 Hz.

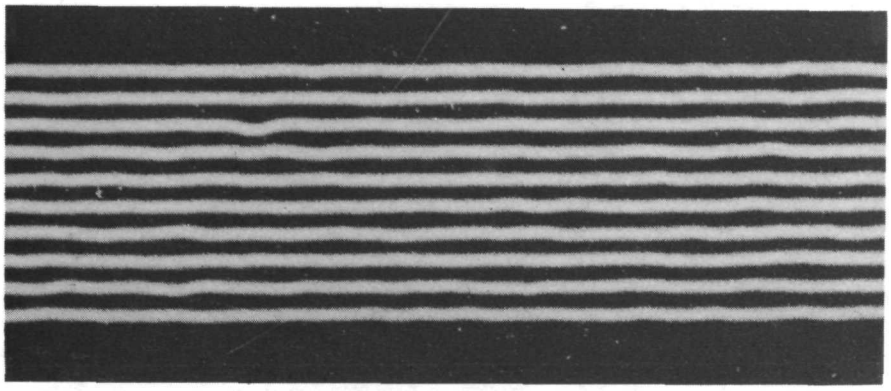

(b) 0.636 arc sec at 0.05 Hz.

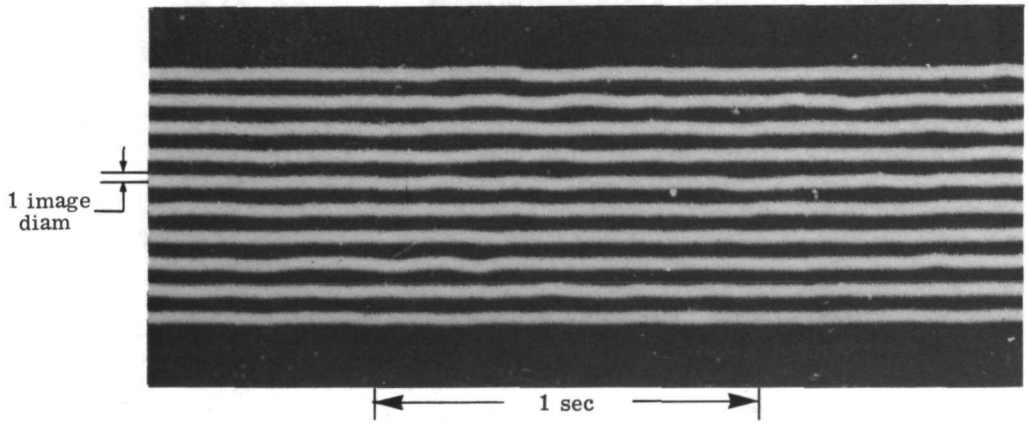

(c) 0.636 arc sec at 0.025 Hz. L-73-6807

Figure 20.- Image stability of fine system to +12.3 magnitude star with image diameter of 107 μm with coarse system being driven sinusoidally at indicated amplitude and frequency.

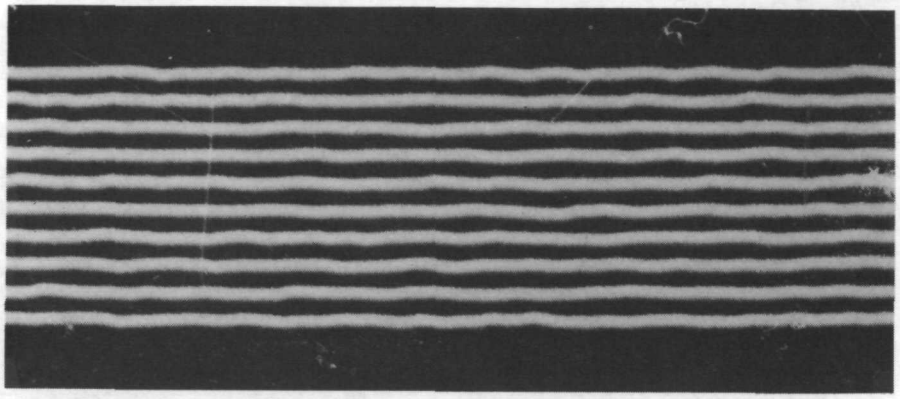

(a) 0.636 arc sec at 0.1 Hz.

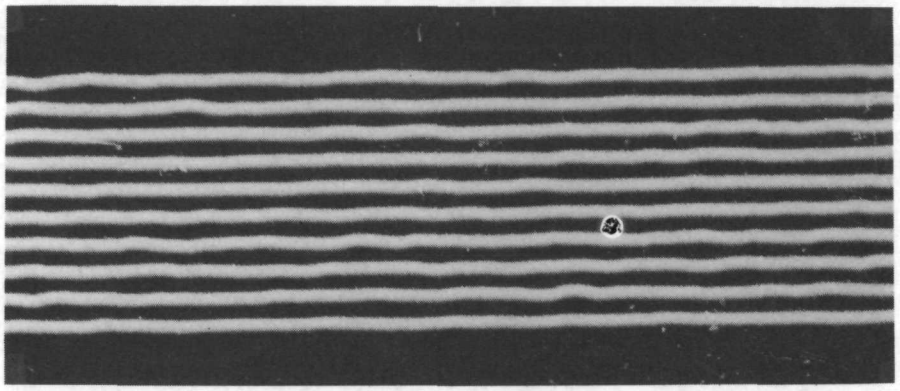

(b) 0.636 arc sec at 0.05 Hz.

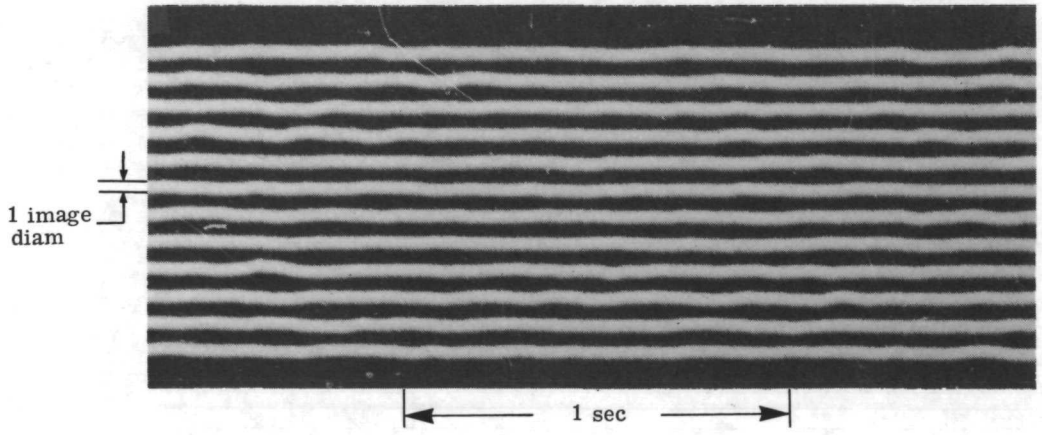

(c) 0.636 arc sec at 0.025 Hz. L-73-6808

Figure 21.- Image stability of fine system to +12.3 magnitude star with image diameter of 188 μm with coarse system being driven sinusoidally at indicated amplitude and frequency.

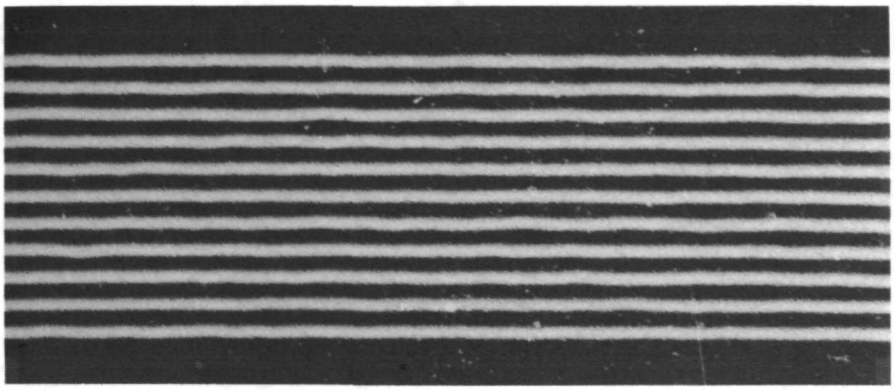

(a) 0.636 arc sec at 0.1 Hz.

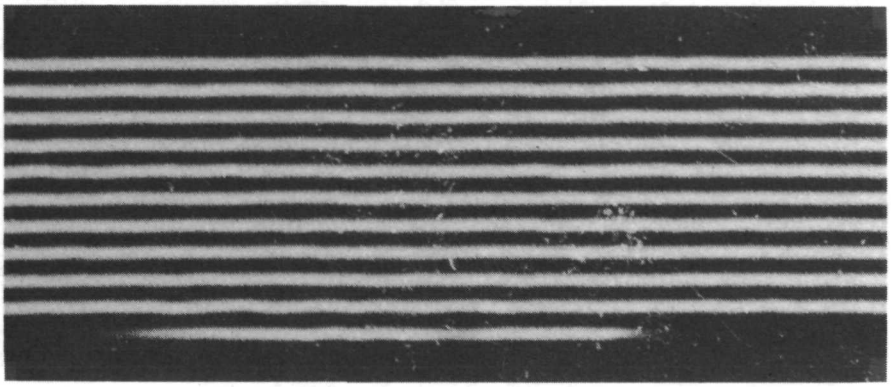

(b) 0.636 arc sec at 0.05 Hz.

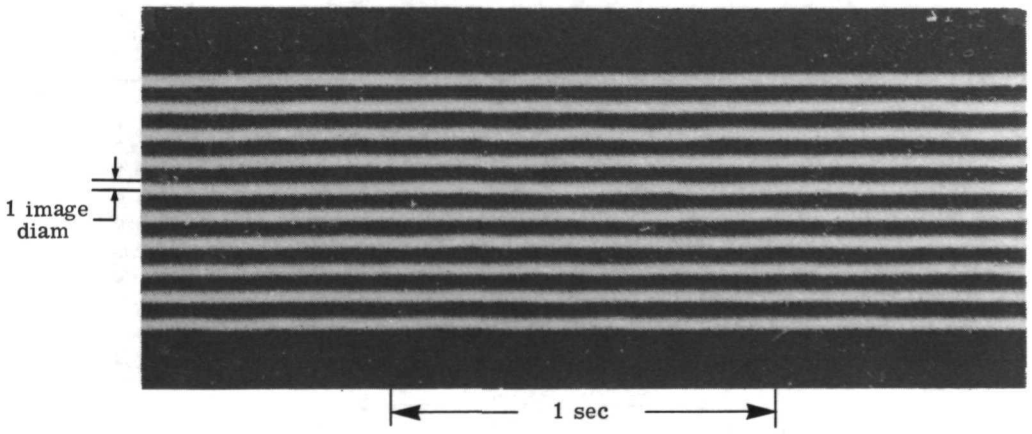

(c) 0.636 arc sec at 0.025 Hz. L-73-6809

Figure 22.- Image stability of fine system to +11.25 magnitude star with image diameter of 107 μm with coarse system being driven sinusoidally at indicated amplitude and frequency.

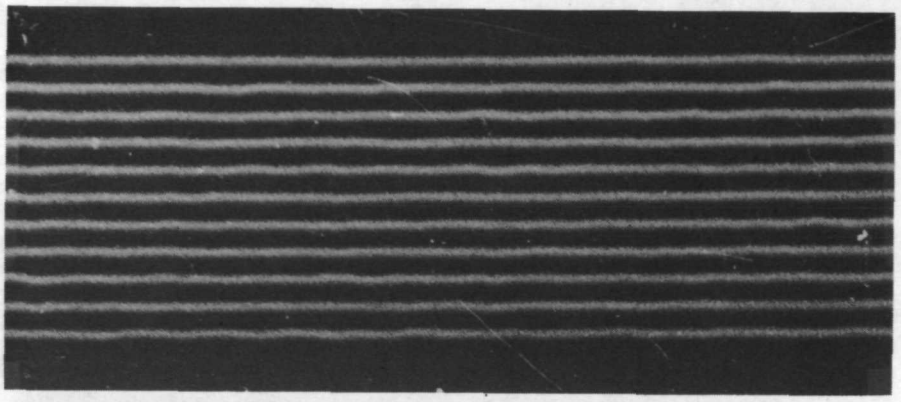

(a) 0.636 arc sec at 0.1 Hz.

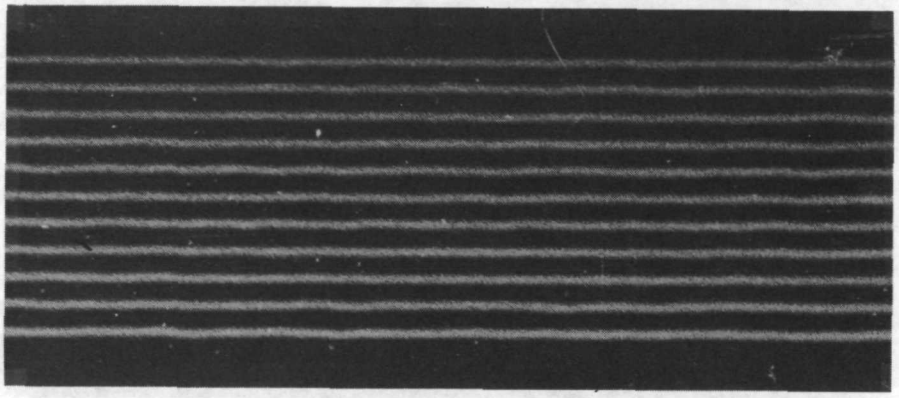

(b) 0.636 arc sec at 0.05 Hz.

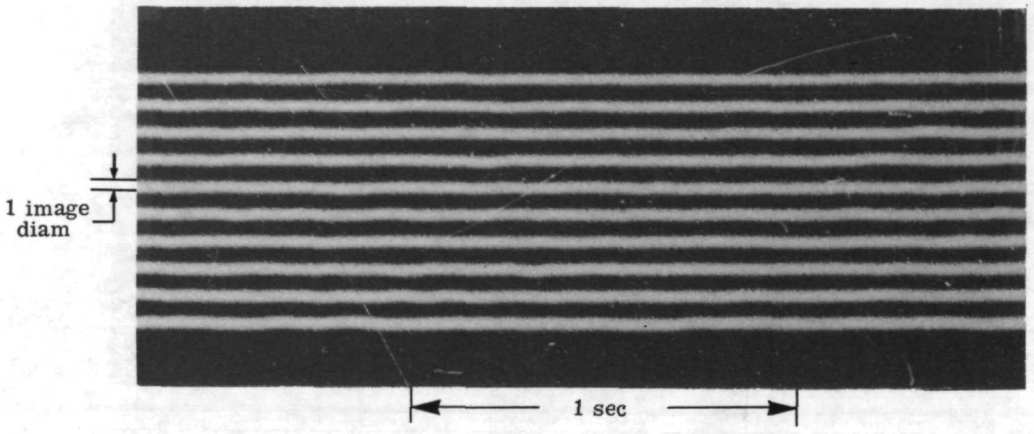

(c) 0.636 arc sec at 0.025 Hz. L-63-6810

Figure 23.- Image stability of fine system to +11.35 magnitude star with image diameter of 188 μm with coarse system being driven sinusoidally at indicated amplitude and frequency.

NASA-Langley, 1973 — 14 L-8943

NATIONAL AERONAUTICS AND SPACE ADMINISTRATION
WASHINGTON, D.C. 20546

OFFICIAL BUSINESS
PENALTY FOR PRIVATE USE $300

SPECIAL FOURTH-CLASS RATE BOOK

POSTAGE AND FEES PAID
NATIONAL AERONAUTICS AND SPACE ADMINISTRATION
451

U.S.MAIL

POSTMASTER : If Undeliverable (Section 158 Postal Manual) Do Not Return

"The aeronautical and space activities of the United States shall be conducted so as to contribute . . . to the expansion of human knowledge of phenomena in the atmosphere and space. The Administration shall provide for the widest practicable and appropriate dissemination of information concerning its activities and the results thereof."

—NATIONAL AERONAUTICS AND SPACE ACT OF 1958

NASA SCIENTIFIC AND TECHNICAL PUBLICATIONS

TECHNICAL REPORTS: Scientific and technical information considered important, complete, and a lasting contribution to existing knowledge.

TECHNICAL NOTES: Information less broad in scope but nevertheless of importance as a contribution to existing knowledge.

TECHNICAL MEMORANDUMS: Information receiving limited distribution because of preliminary data, security classification, or other reasons. Also includes conference proceedings with either limited or unlimited distribution.

CONTRACTOR REPORTS: Scientific and technical information generated under a NASA contract or grant and considered an important contribution to existing knowledge.

TECHNICAL TRANSLATIONS: Information published in a foreign language considered to merit NASA distribution in English.

SPECIAL PUBLICATIONS: Information derived from or of value to NASA activities. Publications include final reports of major projects, monographs, data compilations, handbooks, sourcebooks, and special bibliographies.

TECHNOLOGY UTILIZATION PUBLICATIONS: Information on technology used by NASA that may be of particular interest in commercial and other non-aerospace applications. Publications include Tech Briefs, Technology Utilization Reports and Technology Surveys.

Details on the availability of these publications may be obtained from:

SCIENTIFIC AND TECHNICAL INFORMATION OFFICE

NATIONAL AERONAUTICS AND SPACE ADMINISTRATION

Washington, D.C. 20546